

## **General Disclaimer**

### **One or more of the Following Statements may affect this Document**

- This document has been reproduced from the best copy furnished by the organizational source. It is being released in the interest of making available as much information as possible.
- This document may contain data, which exceeds the sheet parameters. It was furnished in this condition by the organizational source and is the best copy available.
- This document may contain tone-on-tone or color graphs, charts and/or pictures, which have been reproduced in black and white.
- This document is paginated as submitted by the original source.
- Portions of this document are not fully legible due to the historical nature of some of the material. However, it is the best reproduction available from the original submission.

ANALYTICAL AND EXPERIMENTAL STUDY OF A SEPARATION SYSTEM  
FOR TWO SPINNING BODIES ON AN  
ATMOSPHERIC REENTRY TRAJECTORY

By

Nathan D. Watson

Thesis submitted to the Graduate Faculty of the  
Virginia Polytechnic Institute

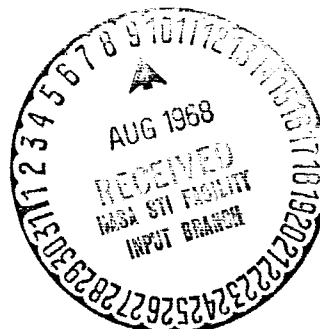
in candidacy for the degree of

MASTER OF SCIENCE

in

Engineering Mechanics

April 1968



FACILITY FORM ONE	N 69-19617	
	(ACCESSION NUMBER)	(THRU)
	73	1
	(PAGES)	(CODE)
	TMX 61533	30
	(NASA CR OR TMX OR AD NUMBER)	(CATEGORY)

ANALYTICAL AND EXPERIMENTAL STUDY OF A SEPARATION SYSTEM  
FOR TWO SPINNING BODIES ON AN  
ATMOSPHERIC REENTRY TRAJECTORY

By

Nathan D. Watson

ABSTRACT

An analytical and experimental solution for determining the longitudinal and transverse separation distances versus time between two hypervelocity spinning atmospheric reentry bodies is presented. The solution presented in this study is for a system consisting of a conical separation spring and two small solid fuel rocket motors. Since the physical parameters are unique to each experimental probe of this type, one specific reentry probe was selected for this study.

Analytical calculations are presented for the initial spring separation and the additional separation provided by the two small solid fuel rocket motors. A trailing wake model is presented based on a literature search, along with a discussion of its applicability to a hypervelocity blunted body. Input parameters for the rocket motor separation system analysis on a high-speed computer are discussed. Supporting test data of the rocket motor gaseous impingement forces in a vacuum are presented.

Vector equations are derived for calculating the longitudinal and transverse separation distances of the two bodies. Resulting body motions and separation distances are presented for the reentry probe selected for this study.

ANALYTICAL AND EXPERIMENTAL STUDY OF A SEPARATION SYSTEM  
FOR TWO SPINNING BODIES ON AN  
ATMOSPHERIC REENTRY TRAJECTORY

by

Nathan D. Watson

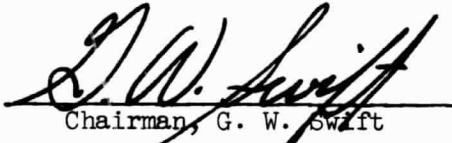
Thesis submitted to the Graduate Faculty of the  
Virginia Polytechnic Institute  
in candidacy for the degree of

MASTER OF SCIENCE

in

Engineering Mechanics

APPROVED:

  
Chairman, G. W. Swift

  
D. H. Pletta

  
H. F. Brinson

  
R. P. McNitt

April 1968

Blacksburg, Virginia

## II. TABLE OF CONTENTS

CHAPTER	PAGE
I. TITLE . . . . .	1
II. TABLE OF CONTENTS . . . . .	11
III. ACKNOWLEDGMENTS . . . . .	1v
IV. LIST OF TABLES AND FIGURES . . . . .	v
V. LIST OF SYMBOLS . . . . .	viii
VI. INTRODUCTION . . . . .	1
VII. ANALYSIS . . . . .	3
A. Problem Definition . . . . .	3
B. Description of Far-Separation System . . . . .	5
C. Description of Trailing Wake . . . . .	6
D. Spring Separation Analysis . . . . .	9
E. Input Parameters for Six-Degree-of-Freedom Computer Program Solution . . . . .	17
F. Gaseous Impingement Problem in a Vacuum Environment . . . . .	21
G. Vector Equations to Calculate Spatial Separation Distances Between Two Bodies . . . . .	22
VIII. RESULTS AND DISCUSSION . . . . .	26
A. Body Orientation and Separation Distances Versus Time . . . . .	26
B. Separation System Verification Test . . . . .	28
C. Discussion . . . . .	29

CHAPTER	PAGE
IX. SUMMARY . . . . .	32
X. BIBLIOGRAPHY . . . . .	33
XI. VITA . . . . .	34

### III. ACKNOWLEDGMENTS

The author wishes to express his indebtedness to Mr. Wilbert C. Falk for his invaluable support in the necessary system tests and his helpful advice in the analytical approach. He is grateful to Miss Kathryn A. Smith for her assistance in the programing of the analytical solutions. The author wishes to thank all other members of the Langley Research Center staff who have aided in the preparation and publication of this manuscript.

In addition, the author wishes to express his appreciation of the valuable comments and advice rendered by his faculty advisor, Dr. G. W. Swift of the Virginia Polytechnic Institute.

#### IV. LIST OF TABLES AND FIGURES

TABLE	PAGE
1. Tabulated Trailing Wake Widths at Several Distances Behind a Blunted Body as Determined in Reference 1 . . .	35
2. Input Parameters for Calculation of Body Motions and Relative Displacements . . . . .	36
3. Vacuum Gaseous Impingement Test Results, Motor Angle of $5^{\circ}$ , Test No. 1 . . . . .	37
4. Vacuum Gaseous Impingement Test Results, Motor Angle of $5^{\circ}$ , Test No. 2 . . . . .	38
5. Vacuum Gaseous Impingement Test Results, Motor Angle of $10^{\circ}$ , Test No. 3 . . . . .	39
6. Total Angle of Attack, Longitudinal and Transverse Separation Distances for Variation of Parameters 10 Seconds After Separation . . . . .	40
FIGURE	
1. Project RAM far separation system . . . . .	41
2. Sequence of events in separation system . . . . .	42
3. Hypersonic trailing wake model for a blunt body . . . . .	43
4. Pressure ratio across the wake at $\frac{X}{D} = 30$ . . . . .	44
5. Project RAM conical separation spring force-deflection curve . . . . .	45
6. Residual thrust curves for X-258 and FW/4S motors . . . . .	46
7. Nominal thrust-time curve for an IKS210 motor at $70^{\circ}$ F . . .	47



FIGURE	PAGE
8. Effective longitudinal thrust-time curve for a motor angle of $5^{\circ}$ , spin rate of 3 revolutions per second, and a delay time of 0.2 second . . . . .	48
9. Effective lateral thrust-time curve for a motor angle of $5^{\circ}$ , spin rate of 3 revolutions per second, and a delay time of 0.2 second . . . . .	49
10. Effective moment-time curve for a motor angle of $5^{\circ}$ , spin rate of 3 revolutions per second, and a delay time of 0.2 second . . . . .	50
11. Separation motor vacuum gaseous impingement test setup . .	51
12. Effective longitudinal thrust-time curve for a motor angle of $5^{\circ}$ , spin rate of 3 revolutions per second, and a delay time of 0.2 second; vacuum impingement effects included . . . . .	52
13. Effective lateral thrust-time curve for a motor angle of $5^{\circ}$ , spin rate of 3 revolutions per second, and a delay time of 0.2 second; vacuum impingement effects included . . . . .	53
14. Effective moment-time curve for a motor angle of $5^{\circ}$ , spin rate of 3 revolutions per second, and a delay time of 0.2 second; vacuum impingement effects included . . . . .	54
15. Geometry of coordinate system used to derive separation equations . . . . .	55

FIGURE	PAGE
16. Total angle of attack versus time for a motor angle of $5^{\circ}$ , spin rate of 3 revolutions per second, and a delay time of 0.2 second . . . . .	56
17. Longitudinal separation distance versus time for a motor angle of $5^{\circ}$ , spin rate of 3 revolutions per second, and a time delay of 0.2 second . . . . .	57
18. Lateral separation distance versus time for a motor angle of $5^{\circ}$ , spin rate of 3 revolutions per second, and a delay time of 0.2 second . . . . .	58
19. Total angle of attack versus time for a motor angle of $5^{\circ}$ , spin rate of 3 revolutions per second, and a delay time of 0.2 second; vacuum impingement effects considered . . . . .	59
20. Longitudinal separation distances versus time for a motor angle of $5^{\circ}$ , spin rate of 3 revolutions per second, and a delay time of 0.2 second; vacuum impingement effects considered . . . . .	60
21. Lateral separation distances versus time for a motor angle of $5^{\circ}$ , spin rate of 3 revolutions per second, and a delay time of 0.2 second; vacuum impingement effects considered . . . . .	61
22. Separation system verification test setup . . . . .	62

## V. LIST OF SYMBOLS

b	slope of residual thrust curve
cg	center of gravity
D	reference diameter
E <sub>s</sub>	spring energy
F <sub>0</sub>	fully compressed spring force
F <sub>1</sub>	maximum residual FW/4S motor thrust
h	altitude
$\hat{i}, \hat{j}, \hat{k}$	unit vectors in the inertial right-hand Cartesian coordinate system
I <sub>x</sub>	roll moment of inertia
I <sub>y</sub>	pitch moment of inertia
I <sub>z</sub>	yaw moment of inertia
K <sub>eff</sub>	effective separation spring constant
l <sub>0</sub>	length of spring stroke
$M = \frac{M_1 + M_2}{M_1 M_2}$	
M <sub>1</sub>	mass of FW/4S motor case
M <sub>2</sub>	mass of experiment package
q	local pressure
q <sub>∞</sub>	free-stream dynamic pressure
$\vec{R}_1$	position vector from earth's center to center of gravity of reentry experiment package
$\vec{R}_2$	position vector from earth's center to center of gravity of FW/4S motor case
$\vec{R}_3 = \vec{R}_2 - \vec{R}_1$	

$\hat{r}_x, \hat{r}_y, \hat{r}_z$	unit vectors in the body centered right-hand Cartesian coordinate system
$r_x(X), r_x(Y), r_x(Z)$	components of the unit vector $\hat{r}_x$
$r_y(X), r_y(Y), r_y(Z)$	components of the unit vector $\hat{r}_y$
$r_z(X), r_z(Y), r_z(Z)$	components of the unit vector $\hat{r}_z$
$s$	Laplace operator function
$T$	residual thrust of FW/4S motor
$t$	time
$t_1$	time for two bodies to come back together after spring separation
$V_1$	velocity vector of reentry experiment package
$X, Y, Z$	earth centered right-hand Cartesian inertial coordinates
$X_s, Y_s, Z_s$	body centered right-hand Cartesian coordinates
$X_1$	generalized coordinate for FW/4S motor
$X_2$	generalized coordinate for the experiment package
$X_1(0)$	displacement of motor case at time zero
$X_2(0)$	displacement of experiment package at time zero
$\bar{X}$	longitudinal separation distance
$\dot{X}$	time derivative of displacement
$\ddot{X}$	time derivative of velocity
$\bar{Y}$	transverse separation distance
$\gamma$	angle between local horizontal and flight velocity vector
$\vec{\omega}$	spin rate

x

$\Gamma_E$	flight-path angle
$\Delta$	heading angle
$\lambda_g$	longitude
$\phi_g$	latitude
$\theta$	separation motor thrust orientation angle
$\Delta t$	delay time between separation motor firings
$\eta$	total angle of attack

## VI. INTRODUCTION

The problem of assuring a clean and continued separation is one which is common to all reentry experimental vehicles which are designed to separate the payload from the burned out last-stage motor just prior to atmospheric reentry. This problem can be divided into two phases: near and far separation. The initial spring separation is referred to as the near separation. The additional impulse required to insure continued separation of the two bodies is provided by the far separation system. The far separation system, in this study, consists of two small solid fuel rocket motors.

Spring energy usually provides an initial relative separation velocity of from 5 to 6 feet per second for the near separation. Since this separation impulse acts along the initial flight path, the velocity vectors of the two bodies after separation lie along the same path. This leaves the burned out motor case trailing in the reentry package wake. As the two bodies enter into the atmosphere and aerodynamic drag increases, the trailing body will rapidly overtake and intercept the reentry package experiment. Thus, an additional system must be provided which will translate the trailing body laterally as well as longitudinally out of the experiment package's wake.

An analytical study of a system using two small solid fuel rocket motors to provide this additional separation is presented. Also, the payload trailing wake and the pressure ratio across the wake behind the body is defined based on a literature search of this problem. The problem of rocket motor exhaust gas impingement in a vacuum is discussed

in general, and test data for a specific problem is presented as it relates to the proposed far-separation system for two spinning bodies. The input parameters for a six-degree-of-freedom computer program solution are discussed. Vector equations, which were added to an existing high-speed six-degree-of-freedom digital computer program and used to determine separation distances versus times, are presented. Calculated transverse and longitudinal separation distances versus time are given for the various cases where such parameters as spin rates and timing delay between separation motor firings have been varied for one specific reentry experiment package separation analysis. Also, calculated results are given for the selected optimum from this study. Finally, the results of a test of the system in an atmospheric environment are presented for a verification of the overall separation system design.

## VII. ANALYSIS

The contents of this chapter have been grouped under seven main headings. First, the problem is defined and is followed by a description of the far-separation system and its operation. Next, the trailing wake of the reentry package experiment is defined based on a literature search. The calculations of the motions resulting from the immediate spring separation, input data for the six-degree-of-freedom computer solution, and an explanation of the gaseous impingement problem in a vacuum with resulting test data are presented in the next three sections. Finally, the vector equations which were added to the existing computer program to calculate the spatial displacements of the two bodies are presented.

### A. Problem Definition

Many of the current hypervelocity atmospheric reentry experiment packages are being designed to be accelerated on an aerodynamic reentry trajectory and then separated from the burned out last-stage motor at a sufficiently high altitude so that no significant aerodynamic drag is present.

Most of the present separation systems provide for only a near separation using primarily spring energy to push the two bodies apart at a relative velocity of from 5 to 6 feet per second. Since the line of action of the spring is along the flight velocity vector, the expended motor case is left trailing in the experiment package's wake. As the bodies enter the atmosphere, the aerodynamic drag builds up, decreasing the leading body's velocity. The trailing motor case, being enveloped



by the reduced pressure of the experiment package's wake, would rapidly overtake and intercept the experiment package. This makes it necessary to provide an additional system to translate the trailing motor case laterally as well as longitudinally out of the leading body's wake. This is referred to as the far-separation system.

The requirement that many of the reentry packages be spin stabilized prior to last-stage separation greatly complicates this problem. Also, most of the rocket motors usually maintain some residual thrusting for several seconds after their nominal burnout time. Since nominal burnout of the last-stage motor usually occurs just a few seconds before atmospheric entry, the initial experiment package-motor case separation must be effected shortly after the nominal burnout. Any system designed for the far separation must be sufficient to account for this residual thrusting and also must translate the last-stage motor case far enough laterally so that it will not interfere with, or reenter, the wake of the experiment package upon atmospheric entry. Also, the far-separation system must be activated almost immediately after the initial spring separation to prevent the expended motor from being driven back into the experiment package by its residual thrust.

The Project RAM reentry experiment probe has been selected for this study. Each atmospheric reentry probe is unique, and the separation system must be tailored to fit the specific problem. Such variables as spin rate, weights, inertias, body shapes, residual motor thrusts, and other design criteria differ for each payload design and prohibit a general solution. However, the approach used here for a solution to a particular atmospheric reentry probe could be utilized in general.

The Project RAM reentry experiment probe was boosted by a four-stage Scout solid fuel vehicle to an altitude of approximately 740,000 feet and then accelerated to nearly 25,600 feet per second by the Scout vehicle's fourth-stage FW/4S motor back on an atmospheric reentry trajectory. This was at an angle of  $-15^{\circ}$  from the horizontal. This experiment package was spin stabilized prior to fourth-stage motor ignition to a nominal spin rate of 3 revolutions per second. Initial spring separation was effected at an altitude of 315,000 feet.

This near-separation impulse was provided by a compressed conical spring whose stored energy was calculated to impart a relative separation velocity between the two bodies of 6.20 feet per second. This energy was released by the firing of two explosive nuts which separated the Marman band mechanical connection between the RAM reentry experiment package and the expended FW/4S Scout motor case.

#### B. Description of Far-Separation System

The far-separation system on the RAM experiment package consisted of two IKS210 solid fuel rocket motors located  $180^{\circ}$  apart on the Delta ring of the FW/4S fourth-stage Scout vehicle. They were oriented to fire in a retro direction with a misalignment of  $5^{\circ}$  off the vehicle thrust axis. This is shown in figure 1.

At the time of separation, the reentry package-FW/4S motor case combination was spinning at 3 revolutions per second. At 0.6 second after the spring separation, the first far-separation motor was ignited which was calculated to impart a coning angle to the expended FW/4S motor

case. Just 0.2 second after the first motor fired, the second far-separation motor was ignited while the first was still thrusting. Together with the timing delay, the two motors provided a backward as well as a transverse component of thrust. This was accomplished at an altitude of 315,000 feet where atmospheric drag was not significant and could be neglected. This was calculated to provide a lateral displacement from the reentry experiment package flight vector sufficient to place the FW/4S motor case out of the disturbing influences of the reentry package's trailing wake before any atmospheric drag was encountered. The preceding events are depicted on figure 2. Timing for the far-separation motor firings was accomplished through the use of delay squib switches which proved to be very accurate for the critical timing delay of 0.2 second between the separation motor firings.

The calculations and tests which were performed to help determine the parameters of the RAM separation system, which were discussed in this section, are presented in sections D, E, and F of the analysis and in section B of the results and discussion.

### C. Description of Trailing Wake

In order to establish a reasonable transverse separation distance between the experiment package and the burned out motor case, it was necessary to define the width of the trailing wake. The first problem was to determine an approximate shape of the wake. It was also desirable to have some definition of the distribution of dynamic pressure within the wake boundaries in order to show that once atmosphere was encountered, the wake pressure would not be sufficient to keep the two bodies apart.

Except at low velocities or very low pressures, atmospheric wakes are turbulent. At the present time, no theory is sufficiently accurate to permit an analytical prediction of the properties of turbulent wakes. Several investigators have added to the experimental knowledge in this field. In reference 2, Dana and Short fired a 0.3125-inch-diameter aluminum sphere into an instrumented ballistic range. Shadowgraphs were taken of the projectile as it passed through a tank evacuated to approximately 10 millimeters of mercury. The results of this study are presented in table 1.

Slattery and Clay reported the results of a similar experiment in reference 12. Their results indicated that turbulence could exist for a distance of 1 mile behind the spherical body.

In reference 5, Feldman shows that the flow about a sphere can be considered as representative of the flow about a blunt body without considering the details of the body geometry as long as the strong bow wave is taken into account. This would permit the direct application of some of the experimental work on spherical bodies to the RAM atmospheric reentry probe.

Scallion, of the NASA Langley Research Center Flight Reentry Programs Office, has attempted to define a wake for a similar-type blunted hypervelocity reentry package. In reference 11 he has defined a wake for a blunted body at a Mach number of 36. This is shown in figure 3. The outer bounds of the wake are the same as the outer bounds of the bow shock. The bow wave was derived from schlieren photographs of a blunted body at a Mach number of 17.6, combined with a faired curve connecting a

straight line representing the asymptotic Mach wave angle. The X and Y coordinates have been normalized by the body diameter. Reference 9, by McCarthy and Kubota, was used to obtain ratios of wake pressure to free-stream dynamic pressure. A prediction of this ratio is shown in figure 4.

A search of some of the available literature on this subject helps to support the approach used in reference 1 to define a turbulent wake for this type problem and is considered sufficiently accurate to be used for this study.

The results presented in figure 3 indicate turbulent wake effects for up to at least four body diameters. For a 2-foot-diameter reentry experiment package, these effects extend to approximately an 8-foot radius in the transverse direction. Also, experimental data in reference 12 indicate that turbulent wake effects can extend up to 1 mile behind the reentry body.

In order to account for some of the uncertainties involved in the wake definition, the far-separation system must provide a safe margin over this transverse wake distance before any significant atmospheric effects are encountered. Another reason for the desirability of a larger transverse separation is to provide for less confusion to the radar experiment package tracking system during atmospheric entry.

The problem of wake definition for hypervelocity reentry bodies is in an early stage of development and involves many interesting problems to be investigated. No attempt has been made to cover this problem in its entirety in this study, but only as it relates to the problem of

providing an adequate separation system for the FW/4S motor case and the RAM reentry experiment package.

#### D. Spring Separation Analysis

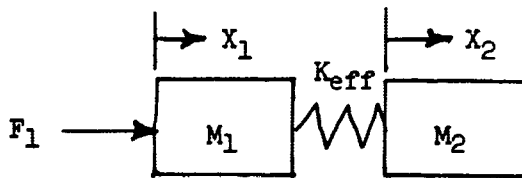
In order to determine the effectiveness of the spring separation system, it was necessary to include the residual thrust of the FW/4S motor in the spring separation analysis. This thrust acts on the system during the action time of the conical spring, and on the FW/4S motor case after the two bodies have been pushed apart by the spring. This residual thrust must be counteracted by the far-separation system before the expended motor case is driven back into the experiment package, making it desirable to calculate the initial relative separation velocity between the two bodies at the instant they separated physically and also to calculate the time they would remain apart without the far-separation system. This determines the time lapse between the initial spring separation and the activation of the far-separation system. The characteristics of the conical spring used on the RAM project are given in figure 5. Total spring energy was obtained by integrating the area under the spring compression curve.

Residual thrust of the FW/4S motor was not easy to define clearly. Each motor exhibits varying magnitudes of residual thrusting after nominal burnout. Residual thrust versus time is presented for three X-258 solid fuel motors and one FW/4S motor in figure 6. These were determined from flight accelerometer readings. Curves from the X-258 motors are presented along with the FW/4S data to help show the variation of residual thrust for several motors. The X-258 is a similar type solid

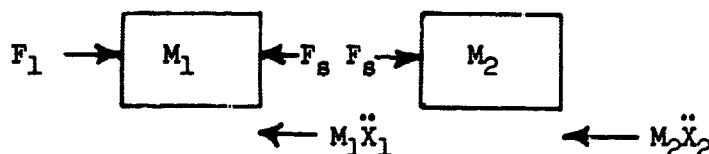
fuel motor, which was replaced by the FW/4S, and thus helps to provide more information on the variation of residual thrust values. These data were used to select the residual thrust-time curve of the FW/4S motor used in this analysis. The top curve shown in figure 6 was selected as the most extreme condition expected and includes a +5-percent increase in thrust values to account for accelerometer accuracy. The parameters used for this analysis are:

Mass of reentry package ( $M_2$ )	$7.98 \frac{\text{lb-sec}^2}{\text{ft}}$
Mass of motor case ( $M_1$ )	$2.84 \frac{\text{lb-sec}^2}{\text{ft}}$
Length of spring stroke ( $l_0$ )	0.417 ft
Total spring energy ( $E_s$ )	32.7 ft-lb
Spring activation time ( $t$ )	0.0732 sec
Fully compressed spring force ( $F_0$ )	230.0 lb
Maximum residual FW/4S motor thrust ( $F_1$ )	30 lb

The system can be represented as follows:



The free-body diagram would then be



Where the spring is initially fully compressed and whose force can be expressed as

$$F_s = F_0 - K_{\text{eff}}(X_2 - X_1)$$

where

$$0 \leq X_2 - X_1 \leq l_0$$

with initial conditions as

$$X_1(0) = X_2(0) = 0$$

$$\dot{X}_1(0) = \dot{X}_2(0) = 0$$

and the equations of motion are

$$M_1 \ddot{X}_1 + F_0 - K_{\text{eff}}(X_2 - X_1) = F_1 \quad (1)$$

$$M_2 \ddot{X}_2 - F_0 + K_{\text{eff}}(X_2 - X_1) = 0 \quad (2)$$

Taking the Laplace transform, these equations become

$$s^2 X_1(s) + \frac{F_0}{sM_1} - \frac{K_{\text{eff}}}{M_1} [X_2(s) - X_1(s)] = \frac{F_1}{M_1 s} \quad (3)$$

$$s^2 X_2(s) - \frac{F_0}{sM_2} + \frac{K_{\text{eff}}}{M_2} [X_2(s) - X_1(s)] = 0 \quad (4)$$

Subtracting equation (3) from equation (4) and letting

$\bar{X}(s) = X_2(s) - X_1(s)$ , this becomes



$$s^2 \bar{X}(s) - \frac{F_0}{s} \left[ \frac{M_1 + M_2}{M_1 M_2} \right] + K_{eff} \left[ \frac{M_1 + M_2}{M_1 M_2} \right] \bar{X}(s) + \frac{F_1}{M_1 s} = 0 \quad (5)$$

Now letting  $M = \frac{M_1 + M_2}{M_1 M_2}$  and solving for  $\bar{X}(s)$  in equation (5)

$$\bar{X}(s) \left[ s^2 + K_{eff} M \right] = \frac{1}{s} \left[ F_0 M - \frac{F_1}{M_1} \right]$$

$$\bar{X}(s) = \frac{F_0 M - \frac{F_1}{M_1}}{s \left[ s^2 + K_{eff} M \right]}$$

Taking the inverse of this yields

$$\bar{X}(t) = \frac{\left( F_0 M - \frac{F_1}{M_1} \right)}{K_{eff} M} \left[ 1 - \cos \sqrt{K_{eff} M} t \right]$$

The spring action time can be determined by solving this equation for  $t$  with  $\bar{X}(t) = l_0$

$$\cos \sqrt{K_{eff} M} t = \left[ 1 - \frac{\left( \bar{X}(t) K_{eff} M \right)}{\left( F_0 M - \frac{F_1}{M_1} \right)} \right]$$

$$t = \frac{1}{\sqrt{K_{eff} M}} \cos^{-1} \left[ 1 - \frac{\left( \bar{X}(t) K_{eff} M \right)}{\left( F_0 M - \frac{F_1}{M_1} \right)} \right]$$

Substituting in the proper values, the spring activation is calculated as

$$t = \frac{1}{\sqrt{(376)(0.477)}} \cos^{-1} \left[ 1 - \frac{\left( (0.417)(376)(0.477) \right)}{\left( (230)(0.477) - \frac{30}{2.84} \right)} \right] 57.3$$

$$t = 0.0732 \text{ sec}$$

Differentiating with respect to  $(t)$  yields

$$\dot{\bar{x}}_t = \frac{\left(F_0 M - \frac{F_1}{M_1}\right)}{\sqrt{K_{\text{eff}} M}} \sin \sqrt{K_{\text{eff}} M} t \quad (6)$$

Since this was a nonlinear conical spring, the total energy  $E_s$  was determined by integrating the area under the spring force deflection curve in figure 5 and solving for an effective spring constant

$$E_s = \frac{1}{2} K_{\text{eff}} l_o^2$$

$$K_{\text{eff}} = \frac{2^{\text{ps}}}{l_o^2} = \frac{2(32.7)}{(0.417)^2} = 376.0 \frac{\text{lb}}{\text{ft}}$$

Now, substituting these values into equation (6), the total relative separation velocity at the instant the spring extends to its free length was found to be

$$\dot{\bar{x}}_{(t)} = \frac{\left[(230)(0.477) - \frac{30}{2.84}\right]}{\sqrt{(376.0)(0.477)}} \sin 56.0^\circ$$

where

$$M = \frac{10.82}{22.7} = 0.477 \frac{\text{ft}}{\text{lb-sec}^2}$$

$$\dot{\bar{x}}_{(t)} = 6.20 \frac{\text{ft}}{\text{sec}}$$

Now, substituting  $\bar{X}(t) = X_2 - X_1$  back into equation (2),  $\dot{X}_2$  can be determined

$$M_2 \ddot{X}_2 - F_0 + K_{eff} \left[ \frac{F_0 M - \frac{F_1}{M_1}}{K_{eff} M} \right] \left[ 1 - \cos \sqrt{K_{eff} M} t \right] = 0$$

$$\ddot{X}_2 = \frac{F_0}{M_2} - \frac{\left[ F_0 M - \frac{F_1}{M_1} \right]}{M M_2} \left[ 1 - \cos \sqrt{K_{eff} M} t \right]$$

Integrating both sides of this equation

$$\dot{X}_2 = \frac{F_0}{M_2} t - \left[ \frac{F_0 M - \frac{F_1}{M_1}}{M M_2} \right] t + \left[ \frac{F_0 M - \frac{F_1}{M_1}}{M M_2} \right] \frac{\sin \sqrt{K_{eff} M} t}{\sqrt{K_{eff} M}} + C_1$$

where

$$X_1(0) = X_2(0) = \dot{X}_1(0) = \dot{X}_2(0) = 0$$

and

$$C_1 = 0$$

$$\dot{X}_2 = \frac{F_0}{M_2} t - \left[ \frac{F_0 M - \frac{F_1}{M_1}}{M M_2} \right] t + \left[ \frac{F_0 M - \frac{F_1}{M_1}}{M M_2} \right] \frac{\sin \sqrt{K_{eff} M} t}{\sqrt{K_{eff} M}} \quad (7)$$

Substituting in the proper values

$$\begin{aligned} \dot{X}_2 &= \frac{(230)(0.0732)}{7.98} - \left[ \frac{(230)(0.477) - \frac{30}{2.84}}{(0.477)(7.98)} \right] 0.0732 \\ &\quad + \left[ \frac{(230)(0.488) - \frac{30}{2.84}}{(0.477)(7.98)} \right] \frac{0.83}{\sqrt{(376)(0.477)}} \end{aligned}$$

$$\dot{x}_2 = 2.13 - 1.95 + 1.57 = 1.75 \frac{\text{ft}}{\text{sec}}$$

$$\dot{x}_1 = \dot{\bar{x}}_t - \dot{x}_2 = 6.20 - 1.75 = 4.45 \frac{\text{ft}}{\text{sec}}$$

Knowing the values of  $\dot{\bar{x}}_t$ ,  $\dot{x}_1$ , and  $\dot{x}_2$  for each body after the immediate spring separation, the following relations for the displacement of each body can be derived

$$M_1 \ddot{x}_1 = T \quad \text{FW/4S motor case} \quad (8)$$

$$M_2 \ddot{x}_2 = 0 \quad \text{Reentry package} \quad (9)$$

Letting the residual thrust be represented by

$$T = T_0 - bt_1$$

and integrating equation (8)

$$d\dot{x}_1 = \frac{T}{M_1} dt_1 = \left[ \frac{T_0}{M_1} - \frac{bt_1}{M_1} \right] dt_1$$

$$\hat{x}_1 = \frac{T_0 t_1}{M_1} - \frac{bt_1^2}{2M_1} + C_1$$

where at

$$t_1 = 0; C_1 = \dot{x}_1 = \dot{x}_1(0)$$

Integrating once more

$$x_1 = \frac{T_0 t_1^2}{2M_1} - \frac{bt_1^3}{6M_1} + x_1(0)t_1 + C_2$$

where at

$$t_1 = 0; C_2 = X_1 = 0$$

$$X_1 = \frac{T_0 t_1^2}{2M_1} - \frac{bt_1^3}{6M_1} + \dot{X}_{1(0)} t_1 \quad (10)$$

Similarly,

$$X_2 = \dot{X}_{2(0)} t_1 + \ddot{X}(t) t_1$$

where the product of the total relative velocity ( $\ddot{X}(t)$ ) between the two bodies and the time ( $t_1$ ) has been added to the expression for  $X_2$ .

The time for the two bodies to come back together in the absence of any additional forces can be determined by equating the expressions for  $X_1$  and  $X_2$  and solving for the time ( $t_1$ ).

$$\frac{T_0 t_1^2}{2M_1} - \frac{bt_1^3}{6M_1} + \dot{X}_{1(0)} t_1 = \dot{X}_{2(0)} t_1 + \ddot{X}(t) t_1$$

Substituting the proper values and solving for ( $t$ ) yields

$$\frac{30t_1^2}{2(2.84)} - \frac{(1.375)t_1^3}{6(2.84)} + 4.45t_1 = 1.75t_1 + 6.20 t_1$$

$$t_1 \left[ t_1^2 - 65.8t_1 + 43.4 \right] = 0$$

$$t_1 = 0.65 \text{ sec}$$

Thus, with a 30-pound residual FW/4S motor thrust, the time for the two bodies to come back together after the initial spring separation is

0.65 second. This determines the requirement that the far-separation system be activated immediately after the initial spring separation.

E. Input Parameters for the Six-Degree-of-Freedom Computer Program Solution

The six-degree-of-freedom digital computer program used to compute the time-varying displacements and body motions of the two bodies in this study is part of a general all-purpose program available for use at the NASA Langley Research Center computer facility. The general moment and acceleration equations are programmed for numerical solutions. Numerical integration of the equations is done by either the Runge-Kutta or the Adams-Moulton methods. Integration intervals can either be constant or controlled automatically by the computer, based on truncation error. Both of these methods are covered in references 4 and 7.

All time-varying forces and moments on the bodies can be input to the program either in tabular or equation form. Interpolation in any table may be performed either linearly, quadratically, or logarithmically and post-multiplied by either an arbitrary constant or any variable computed by the program. For this study, all of the force and moment data were input in tabular form. All other initial position, velocity, and body orientation parameters can be input in either the inertial, earth, geocentric, geodetic, or body reference frames. However, since all computations are carried out in the inertial reference frame, these values are transformed from the reference frame in which they are entered to the inertial reference frame before computation begins.

Position can be specified by either of the following:

- a. Rectangular coordinates relative to the inertial frame.
- b. Altitude, geodetic longitude, and geodetic latitude.
- c. Radial distance from the center of the earth, geocentric longitude, and geocentric latitude.

Velocity can be given by:

- a. Inertial system components of inertial velocity.
- b. Geocentric system of components of inertial velocity.
- c. Geodetic system of components of inertial velocity.
- d. Inertial velocity magnitude and associated path angle and azimuth angle.
- e. Magnitude of velocity relative to the earth, associated path angle, and azimuth angle.
- f. Magnitude of velocity relative to the air, associated path angle, and azimuth angle.

Body orientation can be represented by:

- a. Direction cosines relative to the inertial frame.
- b. Body attitude angle, azimuth angle, and bank angle.
- c. Angle of Attack, angle of sideslip, and bank angle.

The components of the body angular velocity are in the body system.

The program output can be any quantity computed either in the main program or in an appended program. Frequency of output, quantity of output, and, to some extent, format are controlled by the use of input cards. All programming is in FORTRAN language and therefore easier to follow than some of the other machine languages.

The body time-varying angles of attack, inertial velocities, and positions were computed on this main program. The inertial velocities and positions of the two bodies versus time, which was output from the main program, were stored on tape and used as input to the equations presented in section G. These equations, which were added as a subroutine to the main program, were used to compute the spatial transverse and longitudinal separation distances versus time for the two bodies.

A complete derivation of the general acceleration and moment equations, along with the transformation equations, is presented in reference 4. Also, a very complete discussion of the main machine programs, solution techniques, and necessary programing information for the program user is given in some detail. Since this is much too lengthy to be reproduced in this study, the interested program user is referred to the program writeup given in reference 4.

In order to determine the relative time-varying spatial displacements of the burned out fourth-stage FW/4S motor case and the reentry package experiment, it was necessary to define all the external forces and moments acting on the two bodies after separation. Since the separation occurs above any significant atmosphere, there are no aerodynamic disturbances present during the action times of the near- and far-separation systems. Also, after the near-spring-separation system has expended its energy and the two bodies are no longer in physical contact, only the gravitational force acts on the reentry package experiment. This force accounts for equal displacement on both bodies and can be neglected.



The FW/4S motor case has forces resulting from the residual thrust after nominal burnout and the forces and moments of the two IKS210 solid fuel rocket motors of the far-separation system attached to the Delta ring of the expended FW/4S motor case.

The nominal thrust-time curve for an IKS210 motor at room temperature is represented in figure 7. Effective thrust time data were programmed for the proposed far-separation system for a parametric study. Delay times of 0.2 and 0.3 second between the firings of the separation motors were considered. Residual thrust of the FW/4S motor was added to the thrust of the two IKS210 separation motors. Also for these delay times, orientation angles of the IKS210 motors with respect to the FW/4S motor thrust axis of  $0^\circ$ ,  $5^\circ$ , and  $15^\circ$  have been considered. For the nominal case of a  $5^\circ$  motor angle and a delay time of 0.2 second, cases were run for spin rates of 2.5, 3.0, and 3.5 revolutions per second. Typical thrust-time curves for the longitudinal and transverse directions are presented in figures 8 and 9 for a spin rate of 3 revolutions per second, a motor delay firing time of 0.2 second, and a motor orientation angle of  $5^\circ$ . The corresponding moment-time curve for this typical case is presented in figure 10.

The phenomenon of gaseous impingement in a vacuum environment has not been considered in the curves presented in this section. This is accounted for in the following section. The residual thrust curves were presented in part D of this analysis and are not repeated here. The portion of the residual thrust curve which was used in this analysis is noted on figure 6.

#### F. Gaseous Impingement Problem in a Vacuum Environment

In a vacuum environment the flow from a rocket nozzle expands around the nozzle end according to a Prandtl-Meyer expansion. This angle may easily exceed  $90^{\circ}$ . For the case being considered here, this would result in gaseous impingement on the structure of the FW/4S motor case and affect the turning moments and side forces.

A search of several references for methods of calculating the magnitude of this disturbance showed that the calculations would be very involved and the results very questionable. Most of the attempts to correlate calculated and experimental data have been performed with ideal conditions and flat plates as in references 10 and 13. In order to determine the exact exhaust flow field, the source of the flow and all conditions leading up to the flow field must be considered. The chemical products of combustion, the temperature, and the pressure throughout the nozzle and plume flow fields must be known.

For these reasons the most reliable method proved to be a ground test in a vacuum sphere. Reference 10 showed that a valid simulation could be achieved in a test of this type.

A test was set up in the NASA Langley Research Center 60-foot-diameter vacuum sphere. This is shown in figure 11. The boilerplate model of one-half of the FW/4S motor case, with the IKS210 motor mounted at the approximate location as in flight, was mounted on a 704 balance. Also, the base of the experiment package was located at the approximate location as it would be relative to the FW/4S motor case at the time of the separation system activation. This was mounted on a 717 balance,

and forces and moments from both balances were recorded during the separation motor firing. Dashpots filled with heavy oil were attached to the simulated motor case and payload base to slow the system response time and improve the recorded data. Three tests were conducted with the IKS210 motor oriented at  $5^\circ$  to the FW/4S thrust axis in the first two tests and at  $10^\circ$  in the third test. The results of these tests are given in tables 3 through 5.

From the  $5^\circ$  tests, the maximum decrease in turning moment from the exhaust impingement was 18 percent. Data from the 704 balance was questionable for the  $10^\circ$  test. However, the 717 balance recorded a calculated impulse of 0.69 ft-lb-sec for both the  $5^\circ$  and  $10^\circ$  tests.

Data from these tests were utilized to correct the effective thrust and moment curves in figures 8, 9, and 10. These corrected curves are shown in figures 12, 13, and 14.

#### G. Vector Equations to Calculate Spatial Separation

##### Distances Between Two Bodies

The existing six-degree-of-freedom computer program did not contain an option for calculating the relative spatial transverse and longitudinal separation distances between two bodies. These vector equations were added to the existing program as a subroutine to calculate the relative separations. The equations were derived to calculate the longitudinal separation distance along the flight velocity vector and the side or transverse separation distance.

An inertial coordinate system with its origin at the center of the earth was selected. The plus X-axis is located in the equatorial plane

and is pointing at the sun at the time of the vernal equinox. The Y- and Z-axes form the rest of the right-hand Cartesian coordinate system. The geometry of this coordinate system is shown in figure 15. Unit vectors in the X-, Y-, and Z-directions are denoted by  $\hat{i}$ ,  $\hat{j}$ , and  $\hat{k}$ .

Body centered coordinates  $X_s$ ,  $Y_s$ , and  $Z_s$  are located at the center of gravity of the reentry package. The  $X_s$ -axis is in the direction of the flight velocity vector. Unit vectors in the body centered coordinate system are denoted by  $\hat{r}_x$ ,  $\hat{r}_y$ , and  $\hat{r}_z$ . Position vectors for the two bodies are

$$\vec{R}_1 = X_{1i}\hat{i} + Y_{1j}\hat{j} + Z_{1k}\hat{k} \quad \text{Reentry package} \quad (11)$$

$$\vec{R}_2 = X_{2i}\hat{i} + Y_{2j}\hat{j} + Z_{2k}\hat{k} \quad \text{FW/4S} \quad (12)$$

where the velocity of the reentry package can be expressed as

$$\vec{V}_1 = \dot{X}_{1i}\hat{i} + \dot{Y}_{1j}\hat{j} + \dot{Z}_{1k}\hat{k} \quad (13)$$

and the unit vectors in the  $X_s$ -,  $Y_s$ -, and  $Z_s$ -directions are

$$\hat{r}_x = \frac{\vec{V}_1}{|\vec{V}_1|} = \frac{\dot{X}_{1i}\hat{i} + \dot{Y}_{1j}\hat{j} + \dot{Z}_{1k}\hat{k}}{\sqrt{(\dot{X}_1)^2 + (\dot{Y}_1)^2 + (\dot{Z}_1)^2}} \quad (14)$$

$$\hat{r}_y = \frac{\hat{r}_x \times \vec{R}_1}{|\hat{r}_x \times \vec{R}_1|} = \frac{\begin{vmatrix} \hat{i} & \hat{j} & \hat{k} \\ r_x(X) & r_x(Y) & r_x(Z) \\ X_1 & Y_1 & Z_1 \end{vmatrix}}{|\hat{r}_x \times \vec{R}_1|} \quad (15)$$

$$\hat{r}_z = \vec{r}_x \times \vec{r}_y \quad (16)$$

Now expressing  $\hat{r}_x$ ,  $\hat{r}_y$ , and  $\hat{r}_z$  as

$$\hat{r}_x = r_x(X)\hat{i} + r_x(Y)\hat{j} + r_x(Z)\hat{k} \quad (17)$$

$$\hat{r}_y = r_y(X)\hat{i} + r_y(Y)\hat{j} + r_y(Z)\hat{k} \quad (18)$$

$$\hat{r}_z = r_z(X)\hat{i} + r_z(Y)\hat{j} + r_z(Z)\hat{k} \quad (19)$$

and the vector  $\vec{R}_3$  as

$$\vec{R}_3 = \vec{R}_2 - \vec{R}_1 = (X_2 - X_1)\hat{i} + (Y_2 - Y_1)\hat{j} + (Z_2 - Z_1)\hat{k} \quad (20)$$

the separation distances in the  $X_s$ -,  $Y_s$ -, and  $Z_s$ -directions can be expressed by

$$X_s = \vec{R}_3 \cdot \hat{r}_x = (X_2 - X_1)r_x(X) + (Y_2 - Y_1)r_x(Y) + (Z_2 - Z_1)r_x(Z) \quad (21)$$

$$Y_s = \vec{R}_3 \cdot \hat{r}_y = (X_2 - X_1)r_y(X) + (Y_2 - Y_1)r_y(Y) + (Z_2 - Z_1)r_y(Z) \quad (22)$$

$$Z_s = \vec{R}_3 \cdot \hat{r}_z = (X_2 - X_1)r_z(X) + (Y_2 - Y_1)r_z(Y) + (Z_2 - Z_1)r_z(Z) \quad (23)$$

Finally, the desired longitudinal separation distance is expressed as

$$\bar{X} = X_s \quad (24)$$

and the transverse separation distance is

$$\bar{Y} = \sqrt{(Y_s)^2 + (Z_s)^2} \quad (25)$$

These equations were programed as a subroutine to the existing computer program. Values of the  $X_1$ ,  $Y_1$ ,  $Z_1$ ,  $\dot{X}_1$ ,  $\dot{Y}_1$ , and  $\dot{Z}_1$  versus time were taken from the trajectory output for the reentry package on the same program. These data were then programed in tabular form as input to this subroutine. The six-degree-of-freedom program was then run for the separated FW/4S motor case in order to calculate its body motions under the action of all the separation motors and residual thrust forces for each of the cases discussed in sections E and F of this analysis. This subroutine was then called to compute the desired longitudinal and transverse separation distances using the output from the reentry package trajectory and FW/4S motor case computer runs.

Computer data output was obtained in graphical form through the use of a mechanical plotting routine, in addition to the normal printout. These results are presented in Chapter VIII.

## VIII. RESULTS AND DISCUSSION

This chapter is grouped under three main headings. The first section explains the results of this study which are presented in the referenced figures at the end. The next section explains the system verification test and test setup. Finally, a discussion of the results is presented in the last section.

### A. Body Orientation and Separation Distances Versus Time

The reason for this study was to select, analyze, and test an effective separation system for the Project RAM reentry experiment package and the expended FW/4S fourth-stage Scout motor. In preceding sections, the system and the methods of analysis with supporting tests have been presented. The analytical results consist of the predicted time-varying FW/4S body motions under the action of the separation forces along with the longitudinal and transverse separation distances.

Since the aerodynamic effects have been largely neglected in this analysis, the time after separation for which the analysis is valid is approximately 10 seconds. After this the dynamic pressure begins to increase rapidly, resulting in a trailing wake from the leading body, and the analysis no longer holds. At this time, the transverse separation distance must be large enough so that there is no possibility of the FW/4S motor case intercepting the reentry package's trailing wake.

The results presented first are from the parametric study consisting of a series of computer calculations where several parameters have been varied. Delay times between the two IKS210 separation motor firings were

varied from 0.2 to 0.3 second; spin rates were varied from 2.5 to 3.5 revolutions per second. The angle at which the motor is aligned with the thrust axis has been varied between  $0^{\circ}$  and  $15^{\circ}$ . Figures 19, 20, and 21 show the calculated total angles of attack and the X and Y separation distances between the two bodies versus time for a typical case during the first 10 seconds after separation. This is for a separation motor angle of  $5^{\circ}$  with respect to the thrust axis, a timing delay of 0.2 second between motor firings, and a spin rate of 3 revolutions per second. The maximum total angle of attack for the FW/4S motor case along with the longitudinal and transverse separation distances at 10 seconds after separation is given in table 6 for the other cases considered in the parametric study.

The results which have been presented so far have not included the separation motor gaseous impingement effects in a vacuum environment. From these results, a motor angle of  $5^{\circ}$  and a timing delay between the IKS210 motor firings of 0.2 second were selected as the most optimum. This case was then programed and rerun with the resulting force and moment curves in figures 12, 13, and 14, which include the effects of motor exhaust gas impingement in a vacuum. The total angles of attack and the X and Y separation distances versus time are presented in figures 19, 20, and 21 for this case. This shows a calculated longitudinal separation distance of about 760 feet and a transverse separation distance of approximately 820 feet at 10 seconds after separation.

Based on the wake model presented in figure 3, these distances are considered to be more than adequate to insure a continued separation of the two bodies.



### B. Separation System Verification Test

Since the proper functioning of this separation system was essential to the success of the Project RAM reentry package experiment, the system was tested under conditions as close to those in actual flight as possible. In a ground test of the system it was not possible to accurately simulate flight vacuum conditions and gravity forces. However, a free-flight atmospheric ground test was elected as the next best approach for a system verification. This would help to show that the selected timing of 0.2 second between the separation motor firings would result in the motor case achieving a coning angle and translating the body upward and to the side in a spiraling motion as predicted for the flight conditions. Since no expended FW/4S motor cases could be obtained for this test, an available X-258 case was used.

The test hardware consisted of a Scout motor fourth-stage payload adapter, expended X-258 motor case, and an upper D section, all mounted on a ground-secured spin table. Power to drive the spin table was provided by a motor generator. Two of the IKS210 solid fuel separation motors were attached to the upper D section 180° apart. A photograph of the test setup at the NASA Wallops Island Missile Range is shown in figure 22.

Film coverage was provided by four synchronized fixed cameras located 90° apart at a radius of 400 feet from the test setup, and one range tracking camera.

The assembled unit was spun up to approximately 3 revolutions per second by the spin table, and the unit was released from the table by

igniting the explosive nuts of a connecting Marman band. Upon release, the delay squib switches were ignited and a pneumatic piston propelled the unit upward approximately 1 foot above the spin table. The first motor was ignited 0.1 second later, imparting a coning angle to the unit. At 0.2 second from the first motor ignition, the second was ignited. This propelled the unit upward and to the side in a spiraling motion. It reached an approximate height of 80 feet and translated 152 feet to the side into a 6-knot wind and under gravitational forces. Total flight time, as determined from a film frame count, was 4.82 seconds.

### C. Discussion

From the results presented in the two previous sections, the proposed separation system and method of analysis appear to be acceptable. The predicted transverse separation distances for the RAM reentry package and expended FW/4S motor case are sufficient to insure continued separation after they enter the atmosphere. This is based on the predicted trailing wake for a hypersonic blunted atmospheric reentry body shown in figure 3.

The results of a series of calculations of the FW/4S body motions and separation distances versus times for several varying parameters indicate that a good separation can be achieved for all these cases. The system does not involve any de-spin problem and thus results in a more analytically predictable system. Also, looking at the results presented in section A of this chapter, the system proves to be even more effective under the rocket exhaust gaseous impingement effects in a vacuum. Thus, rather than being a problem, the impingement forces

resulting from exhaust gas expansion in a vacuum environment have proved helpful.

Although the residual thrust force of the FW/4S motor could not be simulated in the separation system ground test, the analytical calculations, which included this force, showed that the system is sufficient to account for the most extreme predicted residual thrust.

Some of the inputs to this problem could not be clearly defined as absolute values, such as the residual thrust of the FW/4S motor. Where there was any doubt that these values would be nominal in all cases, the most extreme values were used. This tends to make the analysis more conservative. In the case of gaseous impingement forces in a vacuum, where analytical theory was not considered to be sufficiently developed to provide accurate numbers, a simulated vacuum test was performed and these forces were measured. All time-varying inputs such as forces and moments were programed in tabular form. A sufficient number of points were used to permit an accurate linear interpolation between them by the computer program.

Analytically, this system proves to be by far the most efficient system for this application when compared to other systems considered by other investigators.

This system performed successfully on the first Project RAM reentry experiment probe which was launched from the NASA Wallops Island Launch Facility in October 1967. Initial data analysis of this flight indicates it flew very close to the nominal trajectory. Also, rate gyro and accelerometer flight data at the time of the separation system activation

do not show any unexplained body motions, which indicates the system performed as expected. The initial coning angle was only about  $1^\circ$ . Unfortunately, ground tracking radar failed to provide any data on the expended FW/4S motor case, which prevented the comparison of analytical predictions of separation distances versus time with flight measured. Thus, it can be concluded that the analysis as presented here can be used to accurately predict the performance of a similar system for a similar type payload. However, the input parameters such as weights, inertias, motor residual thrust characteristics, spin rates, and impingement gas forces in a vacuum test must be changed. A major restriction on an experimenter for this type problem is that one must have access to a high-speed computer and a good six-degree-of-freedom digital computer program in order to provide the necessary computational accuracy required.

## IX. SUMMARY

An analytical and experimental solution for determining the longitudinal and transverse separation distances versus time between two hypervelocity spinning atmospheric reentry bodies is presented. Since the varying input parameters are unique to each experimental probe of this type, the Project RAM system was selected for this study.

Analytical calculations are presented for the near-spring separation and the far separation was provided by two small IKS210 solid fuel rocket motors. Supporting test data of the gaseous impingement forces in a vacuum are presented. Input parameters for the far-separation analysis on a high-speed computer are discussed. A trailing wake model is presented based on a literature search, along with a discussion of its applicability to a hypervelocity blunted body. Plotted data are presented for the system by varying parameters, along with the selected optimum system. An attempt has been made to present the analysis in a form such that an experimenter, with a similar type problem on a similar type reentry experiment where the expended last-stage motor is designed to separate from the reentry experiment prior to atmospheric entry, could utilize the approach used here.

## X. BIBLIOGRAPHY

1. Anderson, A. E.: Determination of Sert Payload Separation Tip-Off Impulses and Coning Angle. LTV Contract No. NAS3-2575, Report No. 320.1, November 26, 1962.
2. Dana, T. A.; and Short, W. W.: Experimental Study of Hypersonic Turbulent Wakes. Army Contract No. DA-04-495-ORD-3112, AD258 859, May 29, 1961.
3. Day, W. D.: Tables of Laplace Transforms. London ILIFFE Books Ltd., 1966.
4. Dennison, A. J.; and Butler, J. F.: Missile and Satellite Systems Program for the IBM 7090. Tech. Information Series No. 61 SD 170, Missile and Space Vehicle Dept., General Electric Co., Feb. 1962.
5. Feldman, Saul: On Trails of Axisymmetric Hypersonic Blunt Bodies Flying Through the Atmosphere. Journal of the Aerospace Sciences, vol. 28, June 1961.
6. Greenwood, Donald T.: Principles of Dynamics. Prentice Hall, Inc., 1965.
7. Hildebrand, Francis B.: Advanced Calculus for Applications. Printice Hall, Inc., May 1965.
8. Holl; Maple; and Vinograde: Introduction to the Laplace Transform. Appleton-Century-Crofts, Inc., 1959.
9. McCarthy, John F., Jr.; and Kubota, Toshi: A Study of Wakes Behind a Circular Cylinder at  $M = 5.7$ . AIAA Summer Meeting, Los Angeles, California, No. 63-170, June 1963.
10. Piesik, E. T.; Koppang, R. R.; and Simkin, D. J.: Rocket-Exhaust Impingement on a Flat Plate at High Vacuum. AIAA Paper No. 66-46, January 1966.
11. Scallion, William I.: Approximate Wake Model for the R/P at a Point During the Early Portion of the Reentry Period. FRPO Mission Technical Staff Memorandum, NASA Langley, Hampton, Va., August 2, 1963.
12. Slattery, R. E.; and Clay, W. G.: Width of the Turbulent Trail Behind a Hypervelocity Sphere. Lincoln Lab., Mass: Inst. of Tech., Lexington, Mass., May 17, 1961.
13. Vick, A. R.; and Andrews, E. H., Jr.: An Experimental Investigation of Highly Underexpanded Free Jets Impinging Upon a Parallel Flat Surface. NASA TN D-2326, June 1964.

## XI. VITA

The author was born in [REDACTED]<sup>1</sup>  
[REDACTED] on [REDACTED] [REDACTED] [REDACTED] He graduated from Franklin High School  
near Mt. Airy, North Carolina, in 1953. After attending North Carolina  
State University, Raleigh, North Carolina, for 1 year, he entered the  
U.S. Air Force. After a 4-year tour of duty, he returned to North  
Carolina State University and received the degree of Bachelor of Science  
in Mechanical Engineering in 1962. Since January 1962 he has been  
employed as an Aerospace Engineer by the National Aeronautics and Space  
Administration at the Langley Research Center.

*Nathan D. Watson*

TABLE 1.- TABULATED TRAILING WAKE WIDTHS AT SEVERAL DISTANCES  
BEHIND A BLUNTED BODY AS DETERMINED IN REFERENCE 1

Distance behind projectile, $\frac{X}{D}$	Wake width, $\frac{Y}{D}$
20	1.25
40	2.00
60	2.50
80	2.80
100	3.20
120	3.50
140	3.70
160	3.80
180	3.90
200	4.00
220	4.15
240	4.20



TABLE 2.- INPUT PARAMETERS FOR CALCULATION OF BODY MOTIONS  
AND RELATIVE DISPLACEMENTS

	FW/4S motor	Experiment package
Mass (M), lb-sec <sup>2</sup> /ft	2.84	7.98
Reentry angle ( $\gamma$ ), deg	-15	-15
Separation altitude (h), ft	381,420	381,420
Roll moment of inertia ( $I_x$ ), ft-lb-sec <sup>2</sup>	1.358	3.41
Pitch moment of inertia ( $I_y$ ), ft-lb-sec <sup>2</sup>	11.70	14.512
Yaw moment of inertia ( $I_z$ ), ft-lb-sec <sup>2</sup>	11.70	14.269
Distance to centroid of FW/4S motor from IKS210 motor mounts, ft	1.00	---
Longitude ( $\lambda_g$ ), deg	-63.68	-63.68
Geodetic latitude ( $\phi_g$ ), deg	33.47	33.47
Velocity ( $\vec{V}_1$ ), ft/sec	26,630	26,630
Spin rate ( $\omega$ ), rev/sec	3	3
Flight-path angle ( $\Gamma_E$ ), deg	-14.89	-14.89
Heading angle ( $\psi$ ), deg	118.60	118.60

TABLE 3.- VACUUM GASEOUS IMPINGEMENT TEST RESULTS  
MOTOR ANGLE OF  $5^{\circ}$  - TEST NO. 1

	704 balance	717 balance
Normal load, lb	0	0
Side load, lb	40 (off scale)	2.45
Axial load, lb	214 (maximum) 180 (nominal)	19 (off scale)
Pitch moment, in-lb	0	0
Roll moment, in-lb	63.2	219 (maximum)
Yaw moment, in-lb	2080 (maximum) 1800 (nominal)	55.8 (off scale)

TABLE 4.- VACUUM GASEOUS IMPINGEMENT TEST RESULTS

MOTOR ANGLE 5° - TEST R 2

	704 balance	717 balance
Normal load, lb	0	0
Side load, lb	66.5 (maximum) 46.6 (Nominal)	0.734
Axial load, lb	197 (maximum) 170 (nominal)	11.3
Pitch moment, in-lb	0	0
Roll moment, in-lb	67.5 (maximum) 36 (nominal)	0
Yaw moment, in-lb	1660	82.8

TABLE 5.- VACUUM GASEOUS IMPINGEMENT TEST RESULTS

MOTOR ANGLE OF  $10^{\circ}$  - TEST NO. 3

	704 balance	717 balance
Normal load, lb	0	0
Side load, lb	No data	0
Axial load, lb	186 (maximum) 158 (nominal)	15.1 (maximum) 10.7 (nominal)
Pitch moment, in-lb	0	3.5
Roll moment, in-lb	99	0
Yaw moment, in-lb	555 (questionable)	82.8

TABLE 6.- TOTAL ANGLE OF ATTACK LONGITUDINAL AND  
TRANSVERSE SEPARATION DISTANCES FOR VARIATIONS  
OF PARAMETERS 10 SECONDS AFTER SEPARATION

Spin rate (rev/sec)	Motor angle (deg)	Time delay (sec)	Total angle of attack (deg)	Longitudinal distance (ft)	Transverse distance (ft)
3	0	0.2	35	660	775
3	0	.3	40	820	385
3	5	.2	38	590	760
3	5	.3	30	900	420
3	15	.2	40	450	715
3	15	.3	32	1,020	450
2.5	5	.2	60	310	900
3.5	5	.2	38	805	490

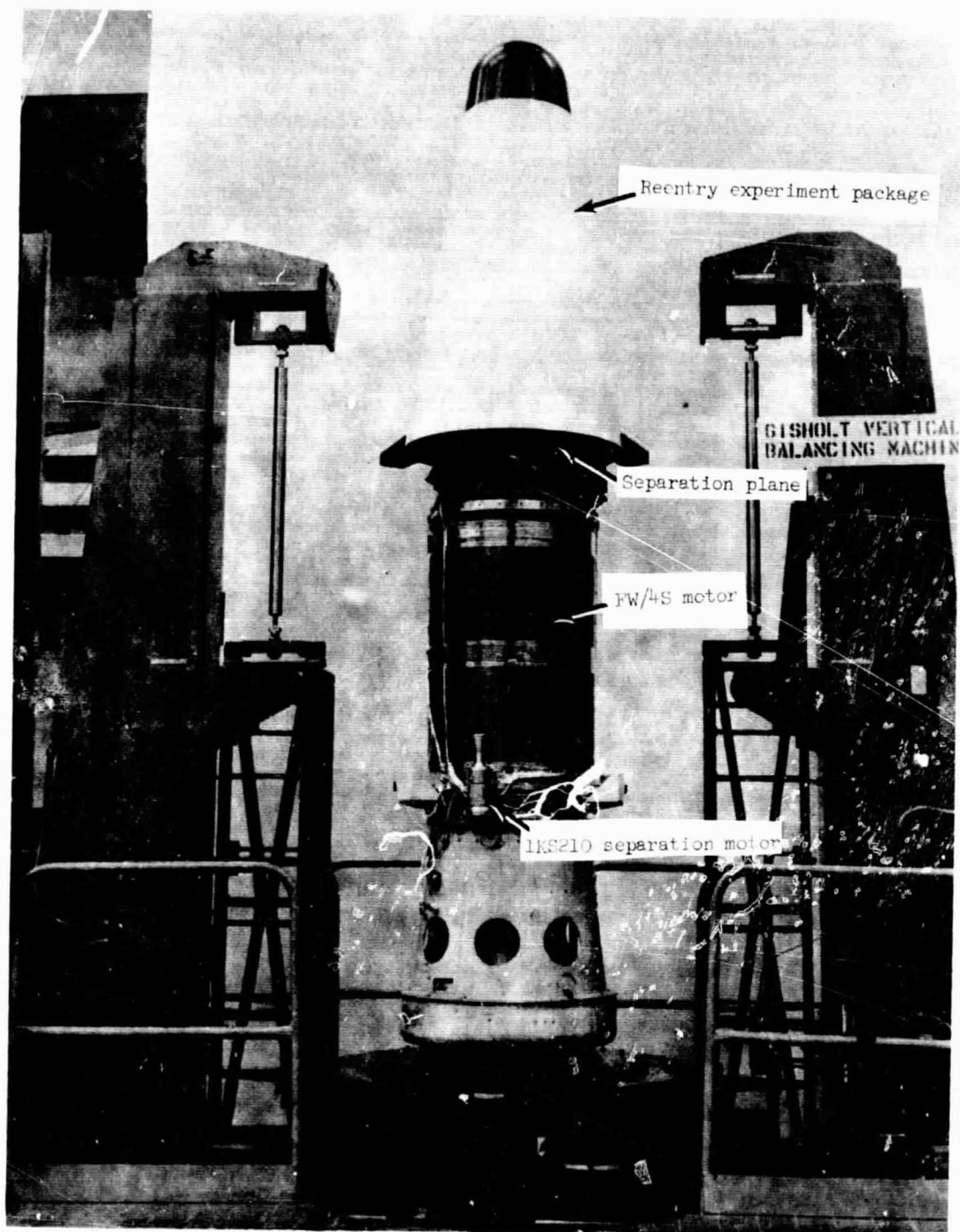


Figure 1.- Project RAM far separation system.

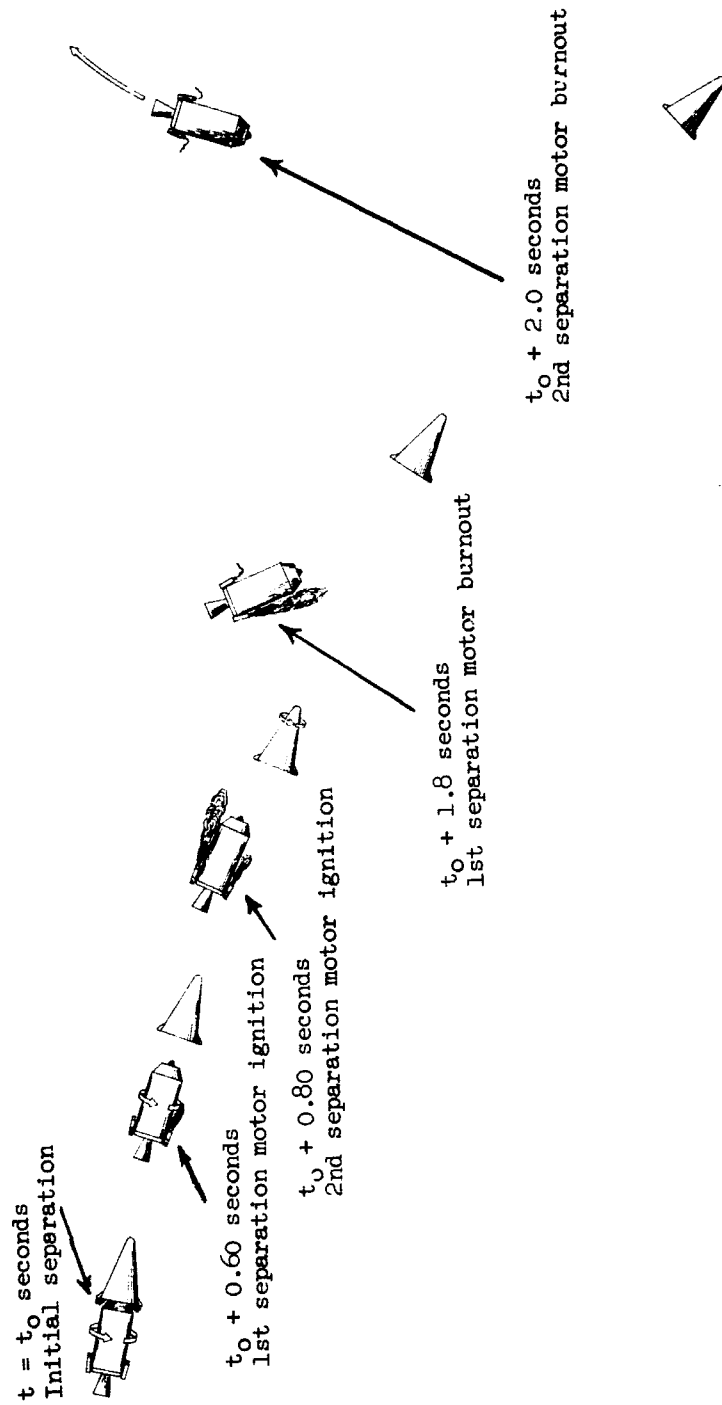


Figure 2.- Sequence of events in separation system.

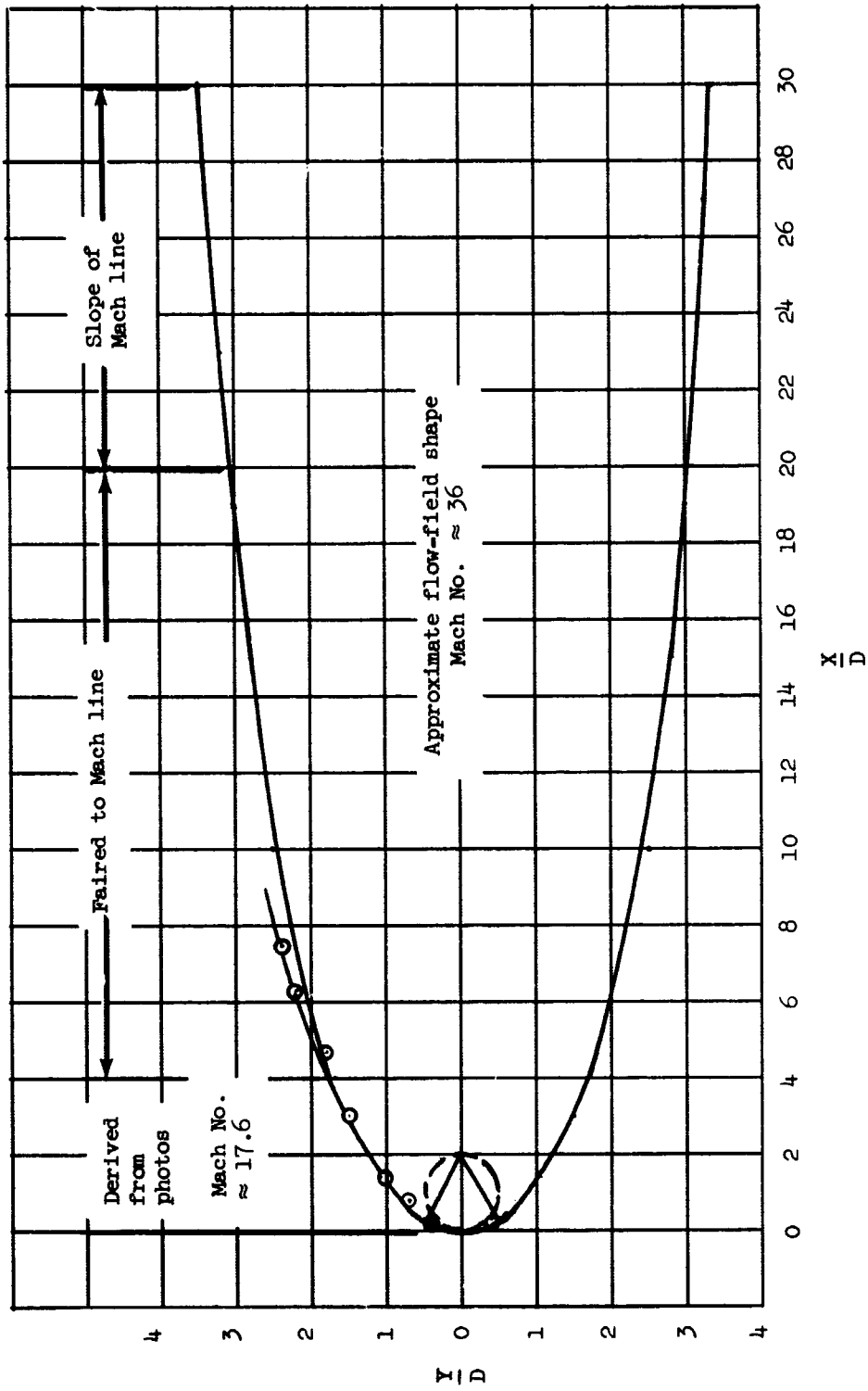


Figure 3.- Hypersonic trailing wake model for a blunt body.



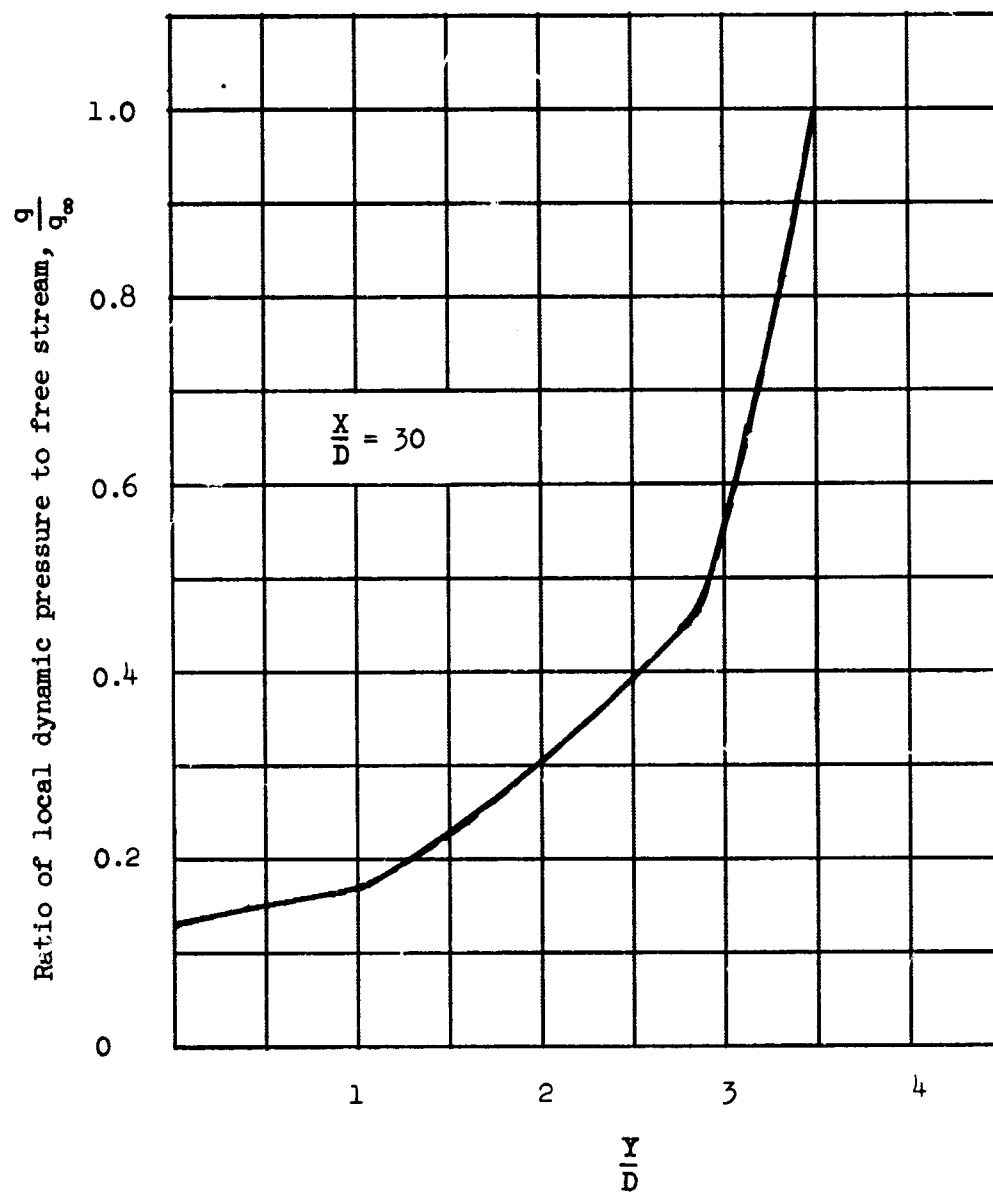


Figure 4.- Pressure ratio across the wake at  $\frac{X}{D} = 30$ .

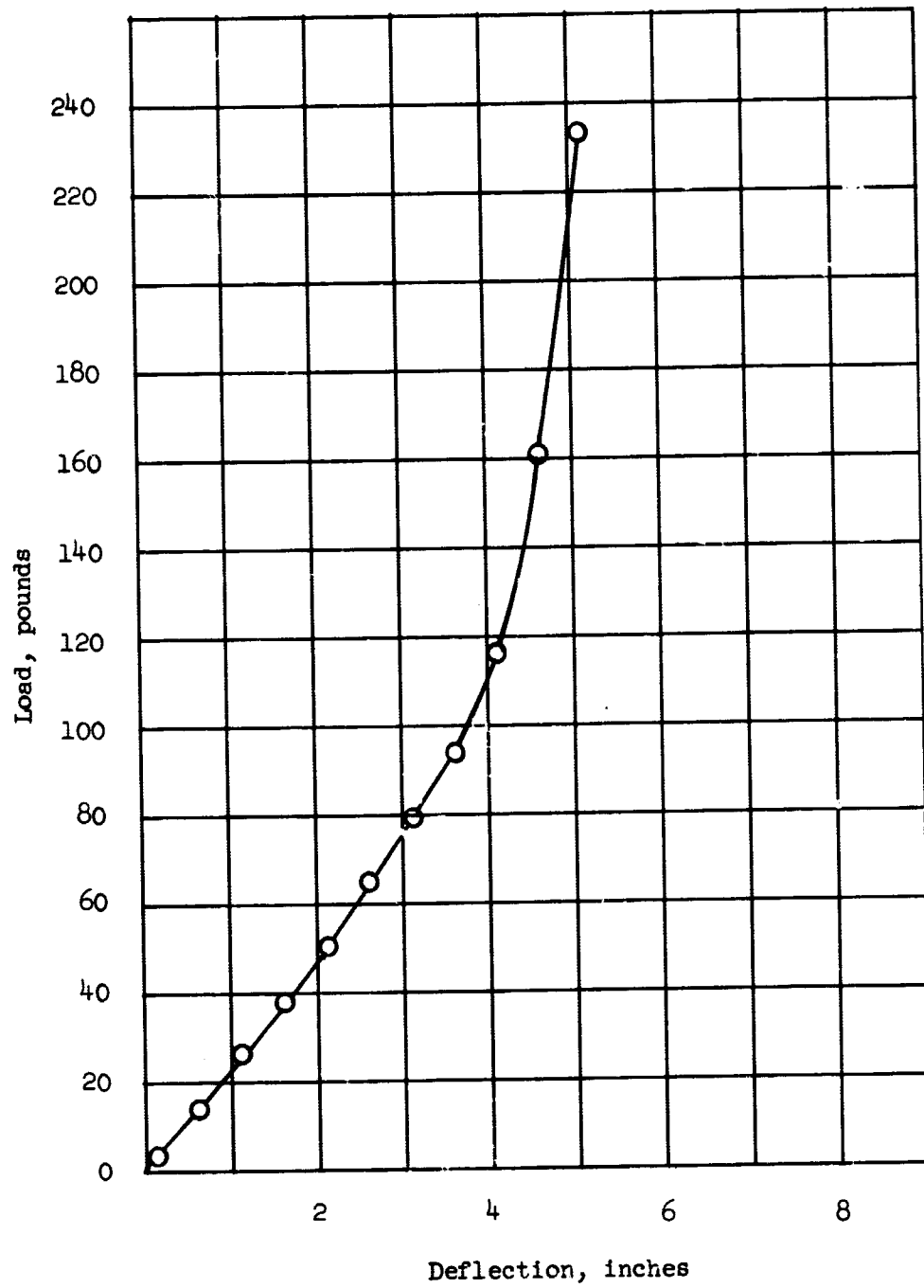


Figure 5.- Project RAM conical separation spring force-deflection curve.

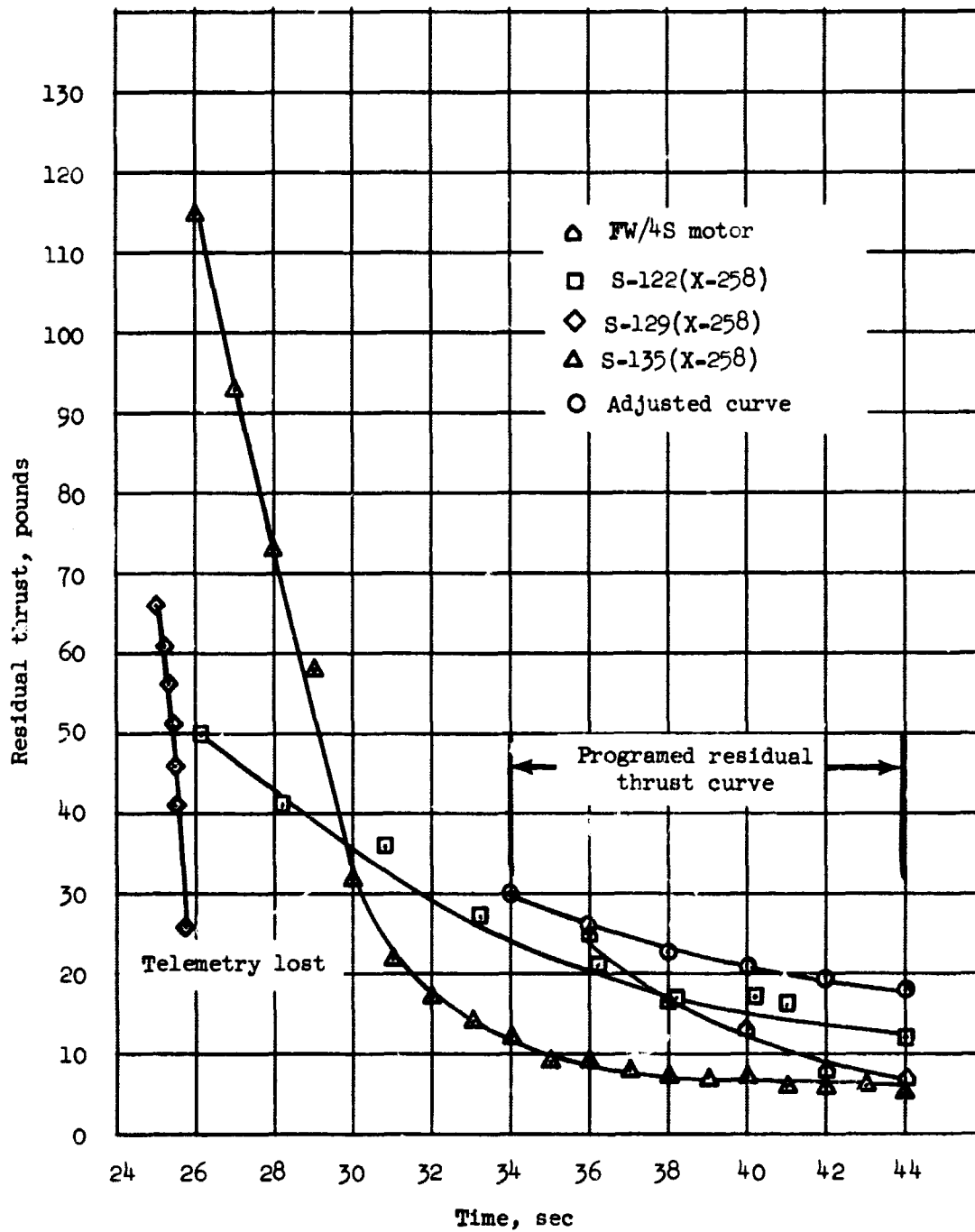


Figure 6.- Residual thrust curves for X-258 and FW/4S motors.

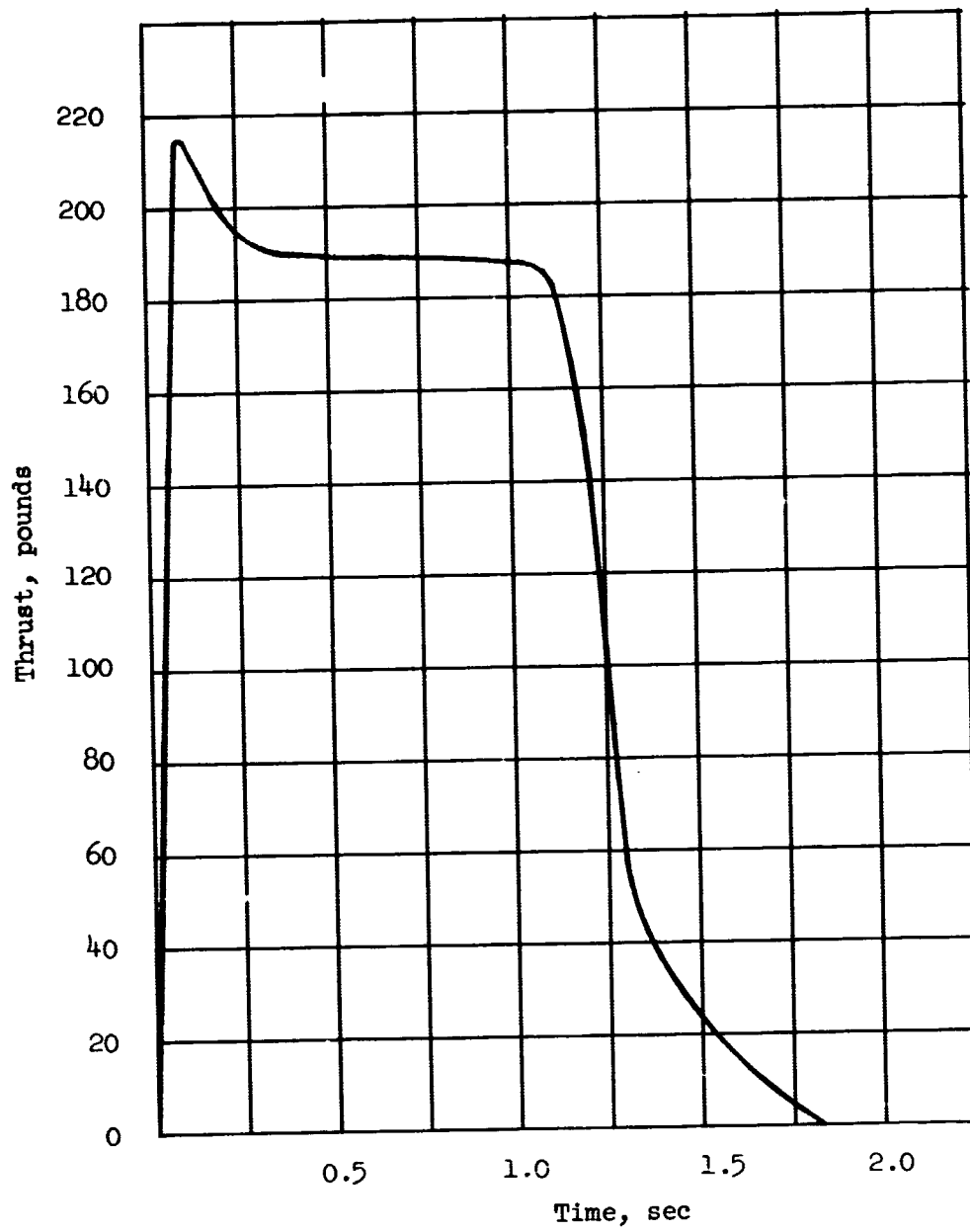


Figure 7.- Nominal thrust-time curve for an IKS210 motor at 70° F.

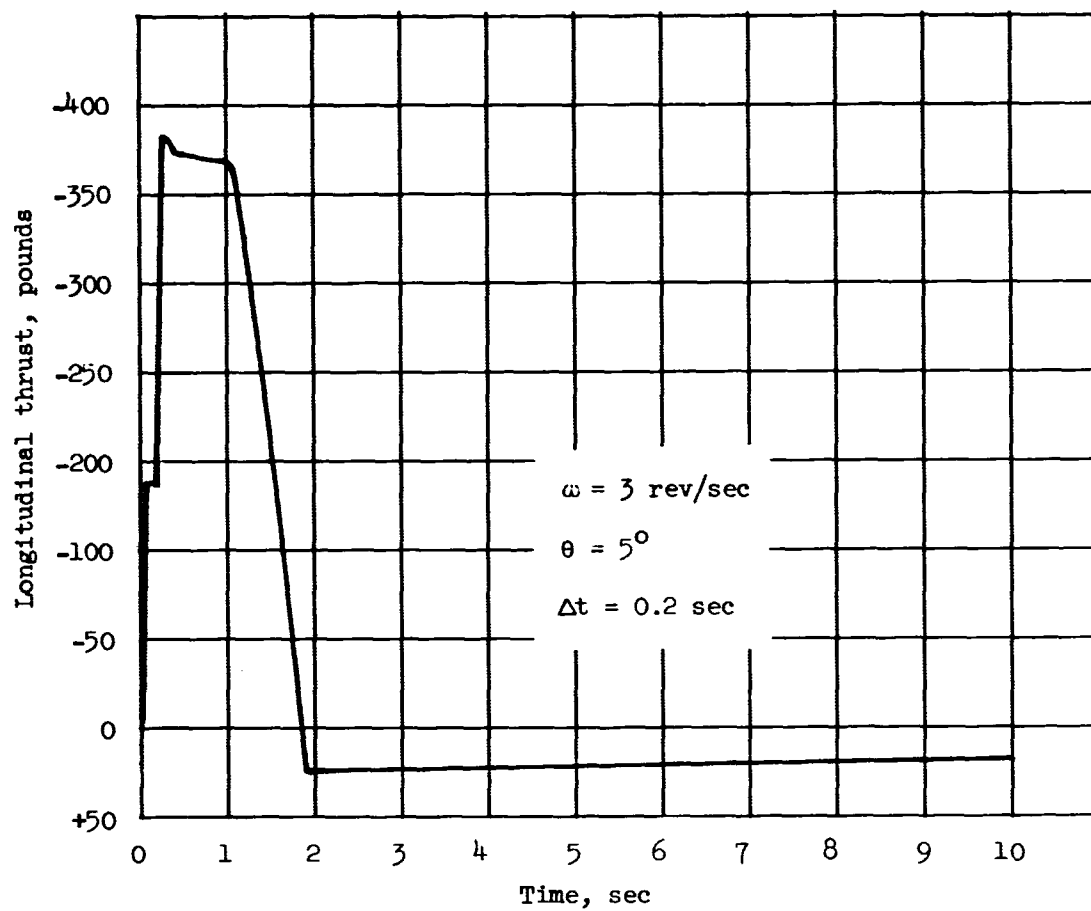


Figure 8.- Effective longitudinal thrust-time curve for a motor angle of  $5^\circ$ , spin rate of 3 revolutions per second, and a delay time of 0.2 second.

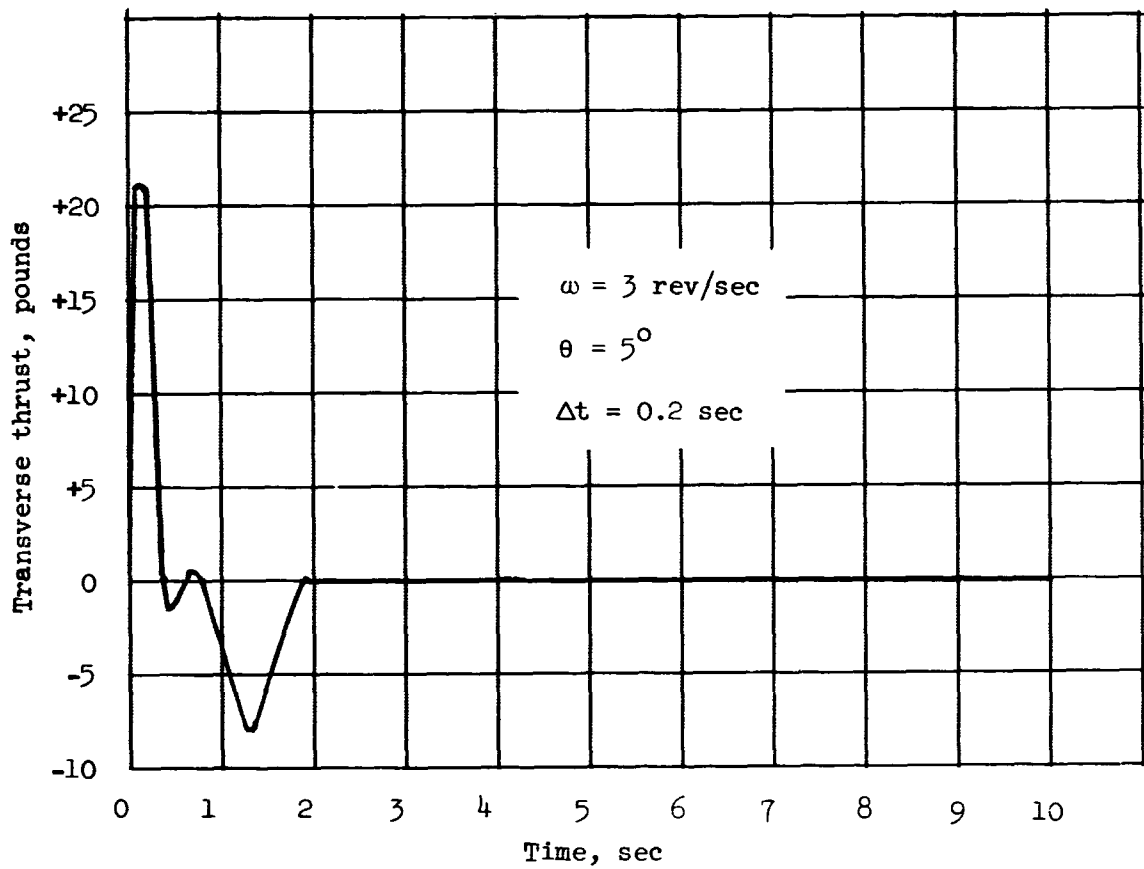


Figure 9.- Effective lateral thrust-time curve for a motor angle of  $5^\circ$ , spin rate of 3 revolutions per second, and a delay time of 0.2 second.

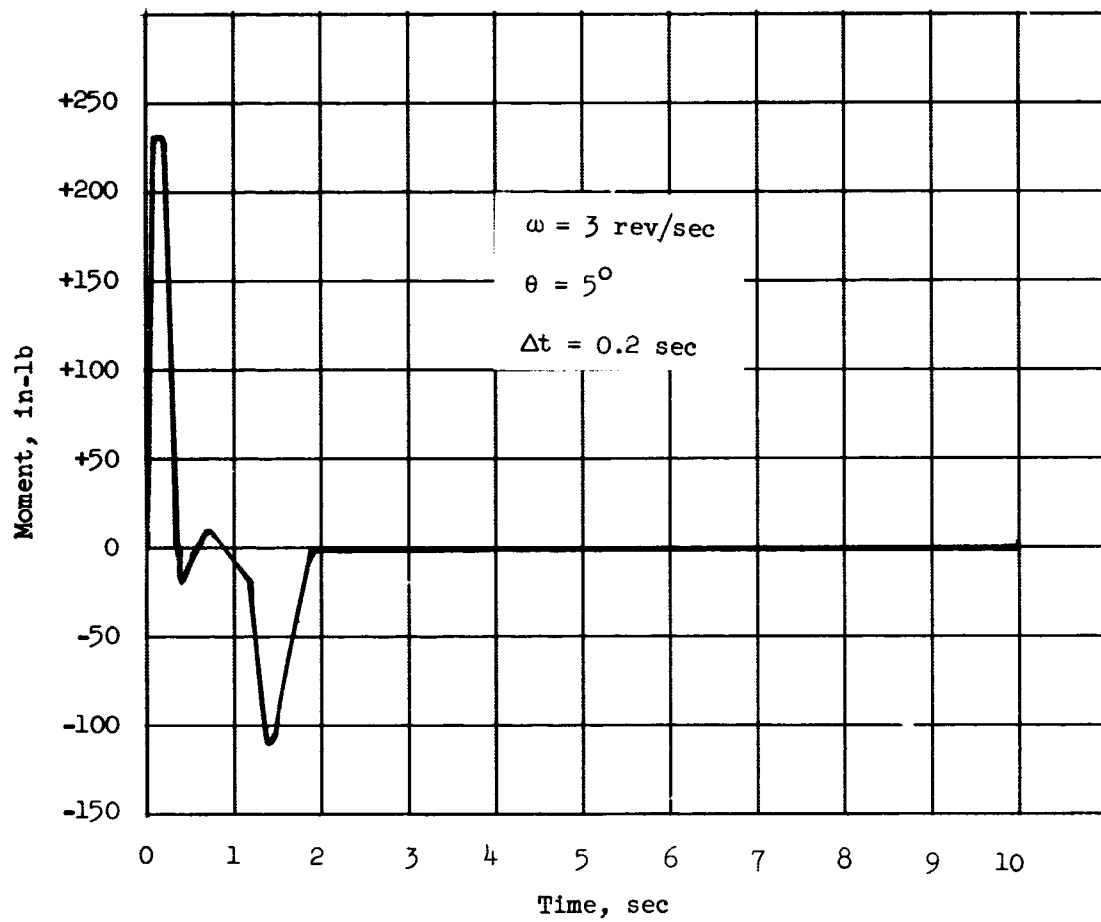


Figure 10.- Effective moment-time curve for a motor angle of  $5^\circ$ , spin rate of 3 revolutions per second, and a delay time of 0.2 second.

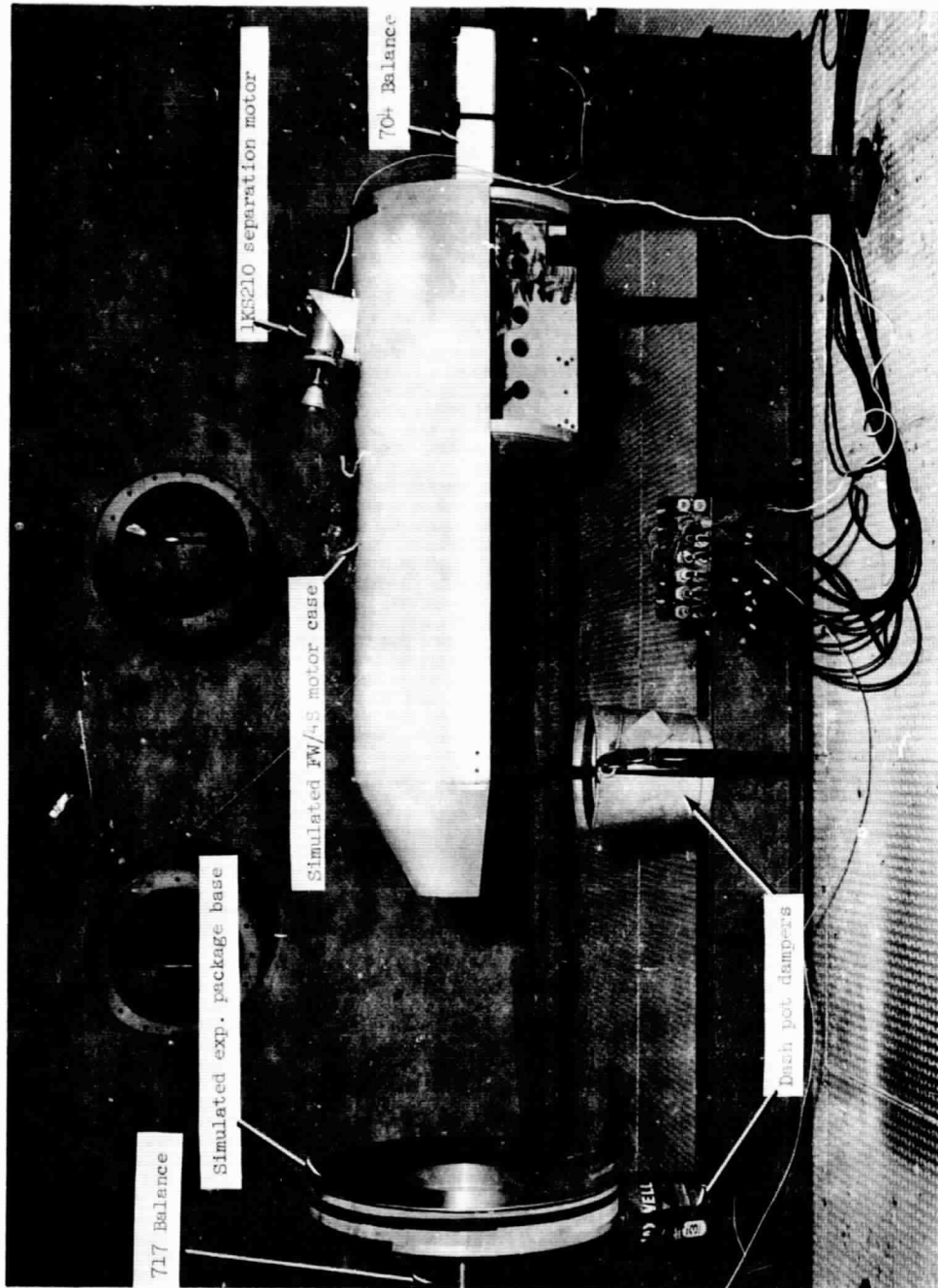


Figure 11.- Separation motor vacuum gaseous impingement test setup.



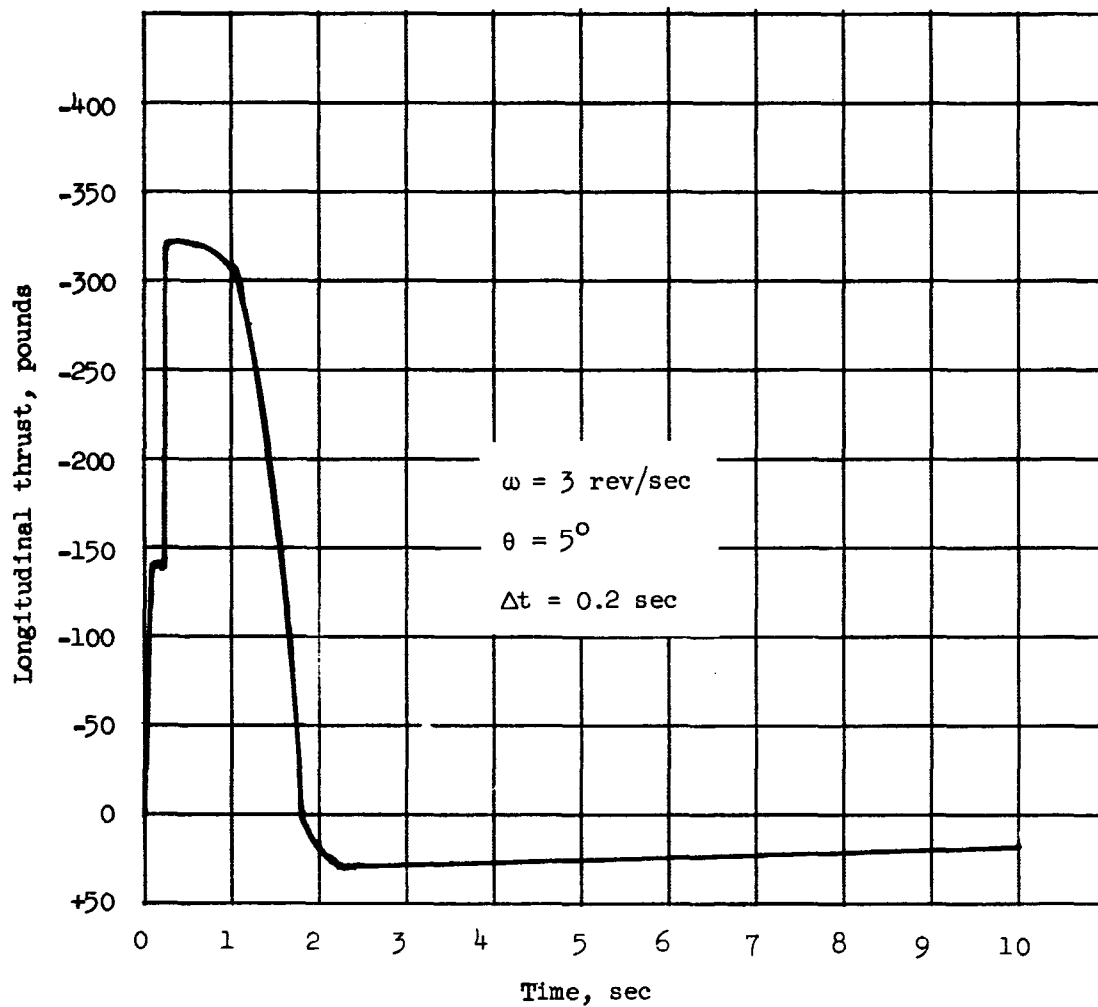


Figure 12.- Effective longitudinal thrust-time curve for a motor angle of  $5^\circ$ , spin rate of 3 revolutions per second, and a delay time of 0.2 second; vacuum impingement effects included.

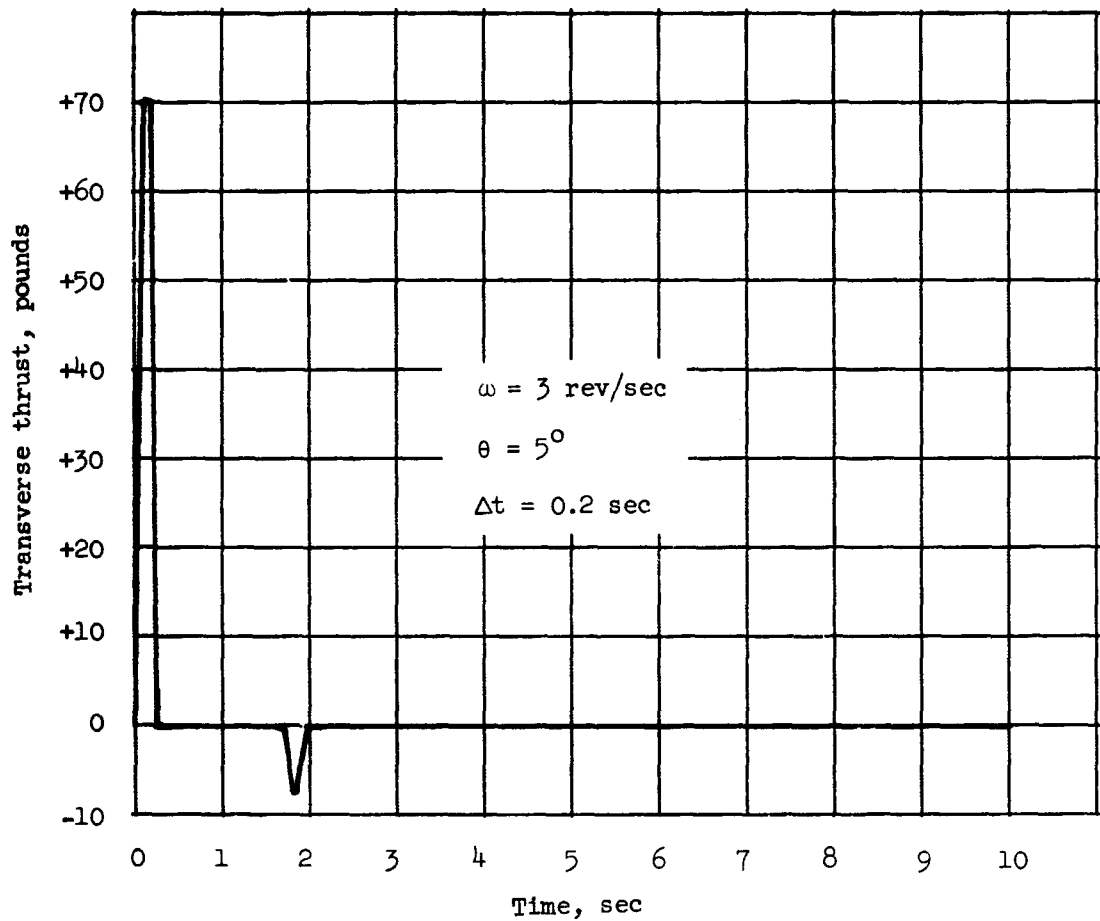


Figure 13.- Effective lateral thrust-time curve for a motor angle of  $5^\circ$ , spin rate of 3 revolutions per second, and a delay time of 0.2 second; vacuum impingement effects included.

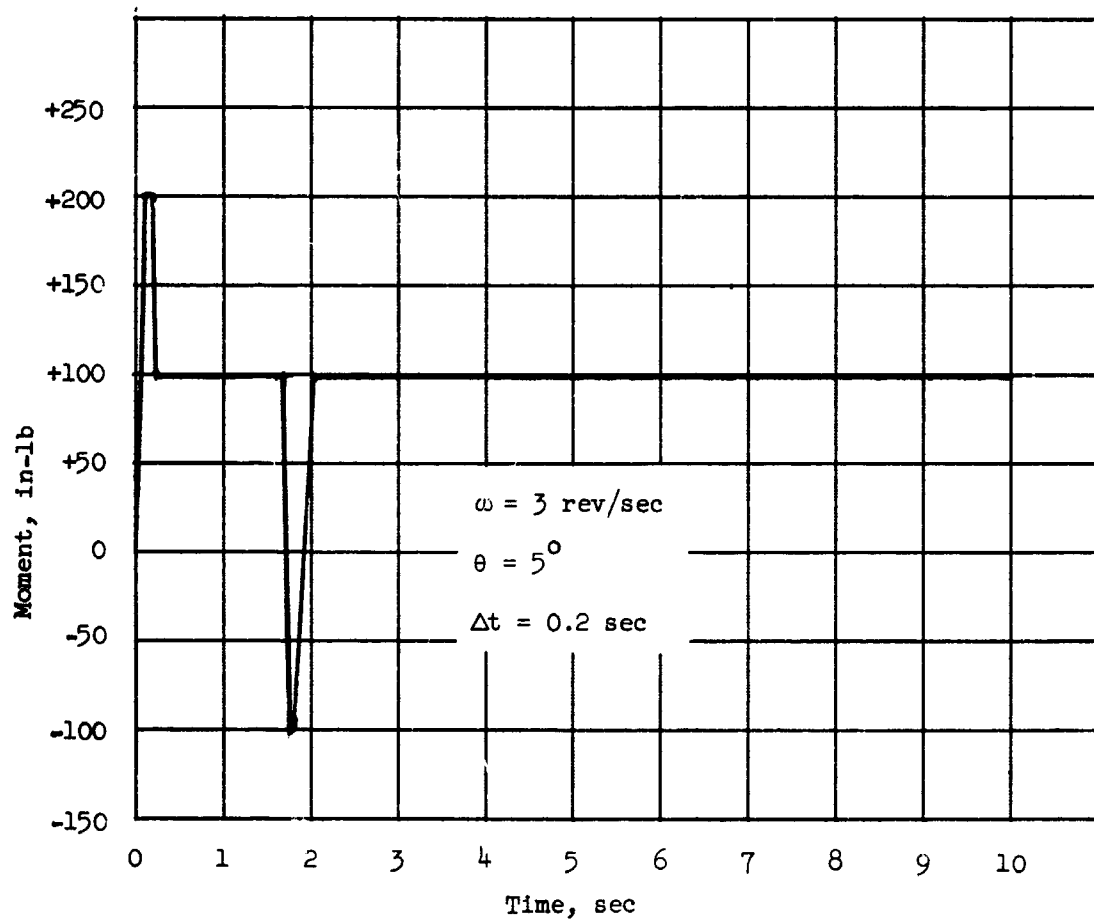


Figure 14.- Effective moment-time curve for a motor angle of  $5^\circ$ , spin rate of 3 revolutions per second, and a delay time of 0.2 second; vacuum impingement effects included.

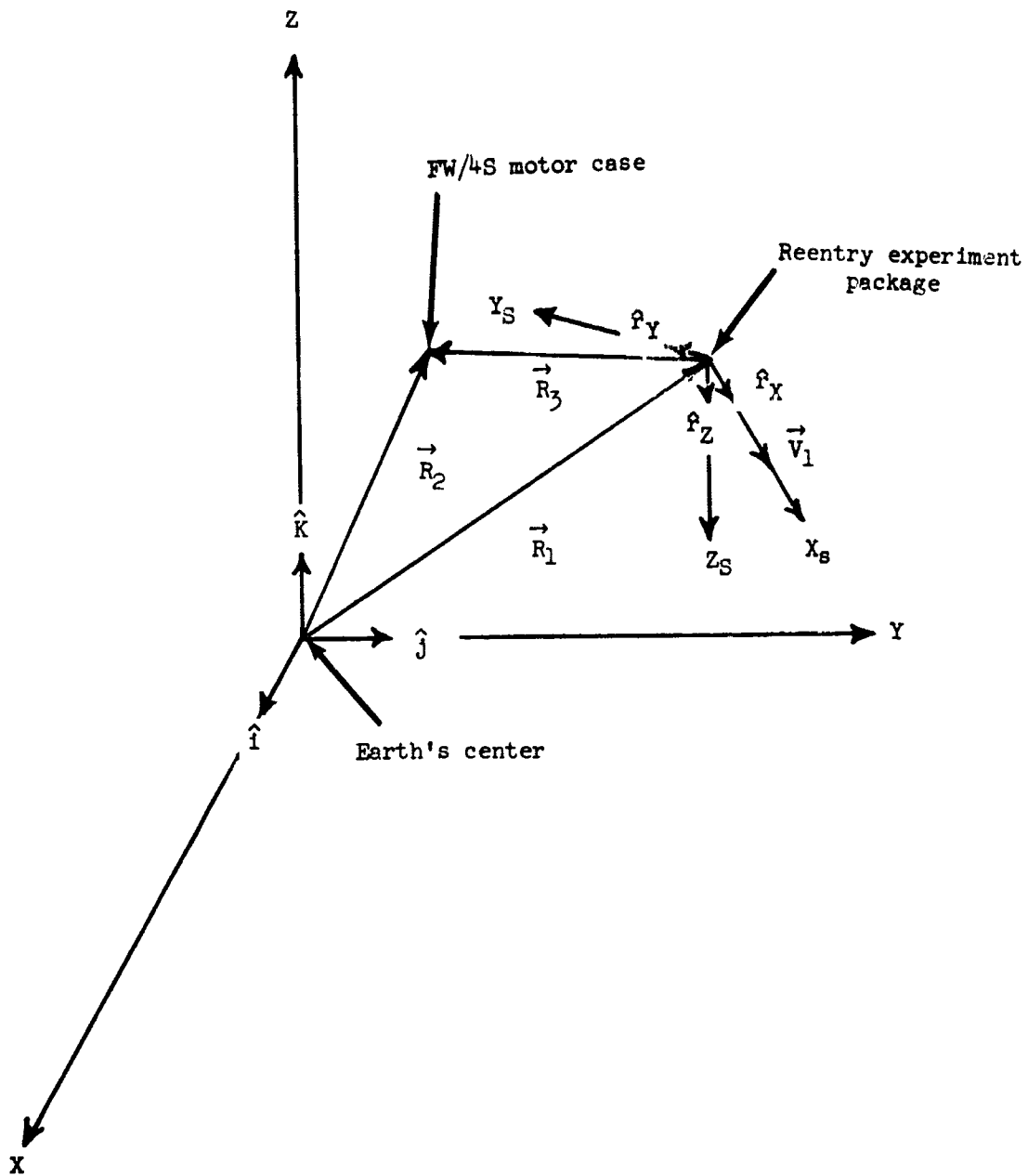


Figure 15.- Geometry of coordinate system used to derive separation equations.

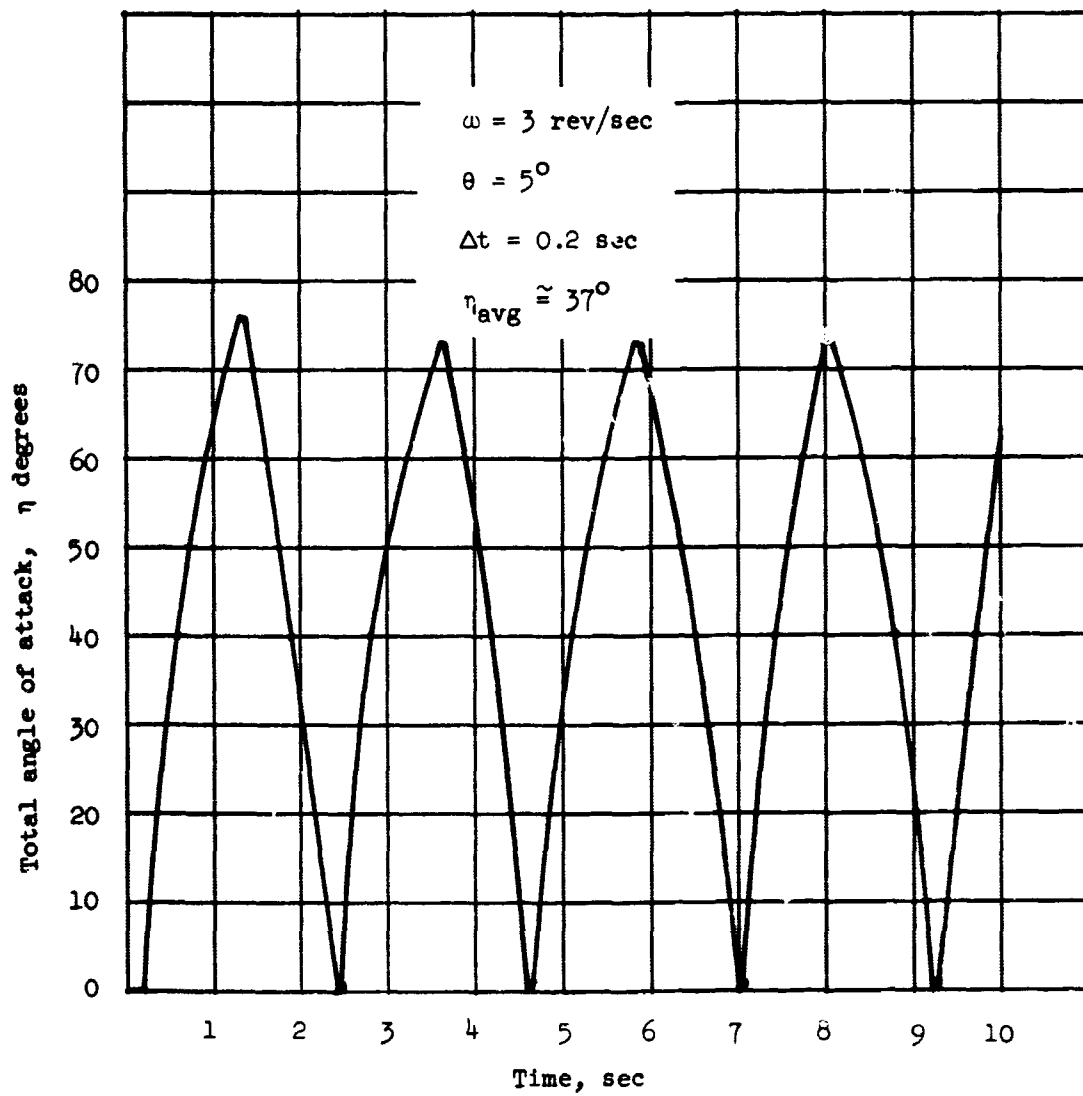


Figure 16.- Total angle of attack versus time for a motor angle of  $5^\circ$ , spin rate of 3 revolutions per second, and a time delay of 0.2 second.

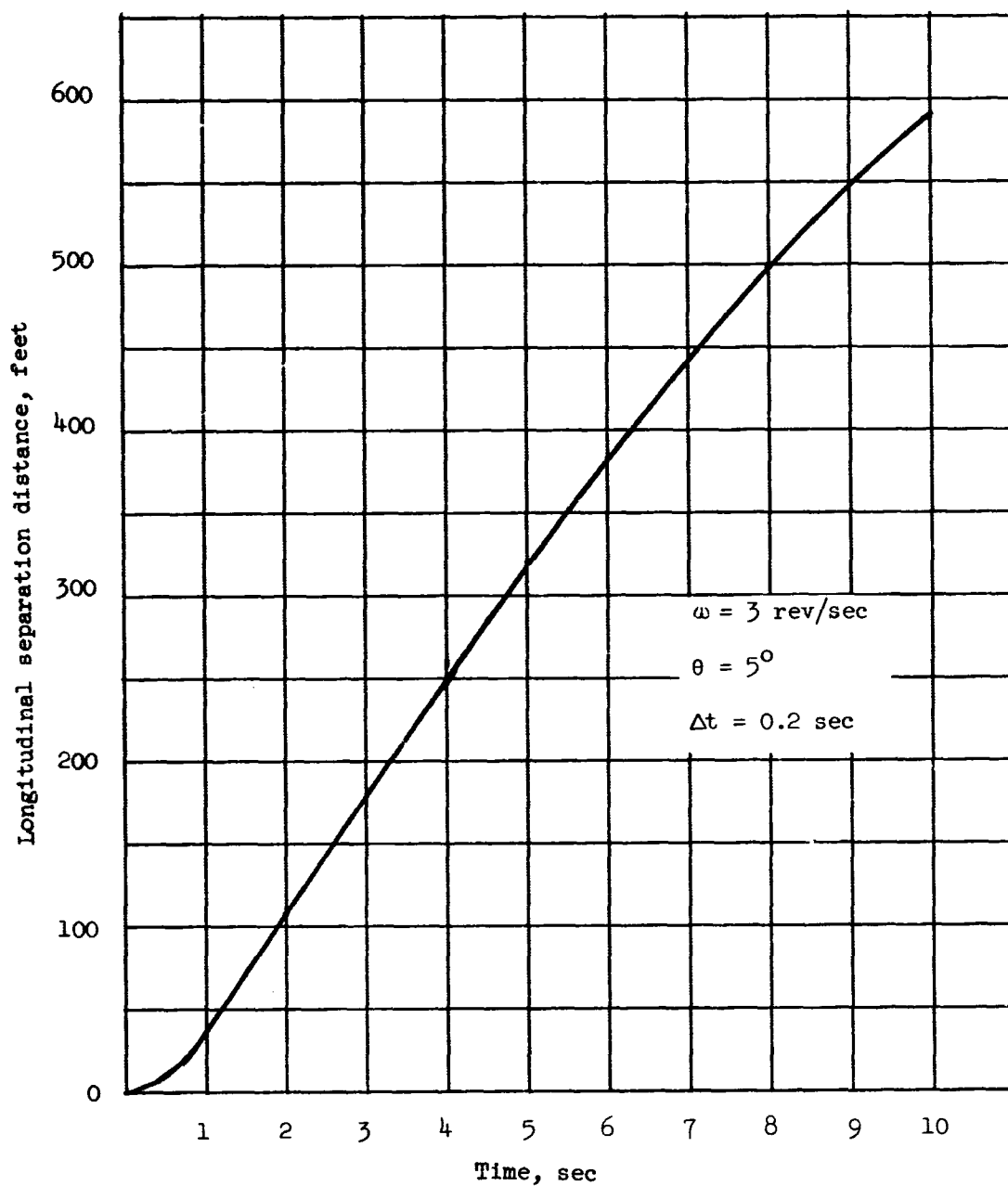


Figure 17.- Longitudinal separation distance versus time for a motor angle of  $5^\circ$ , spin rate of 3 revolutions per second, and a delay time of 0.2 second.

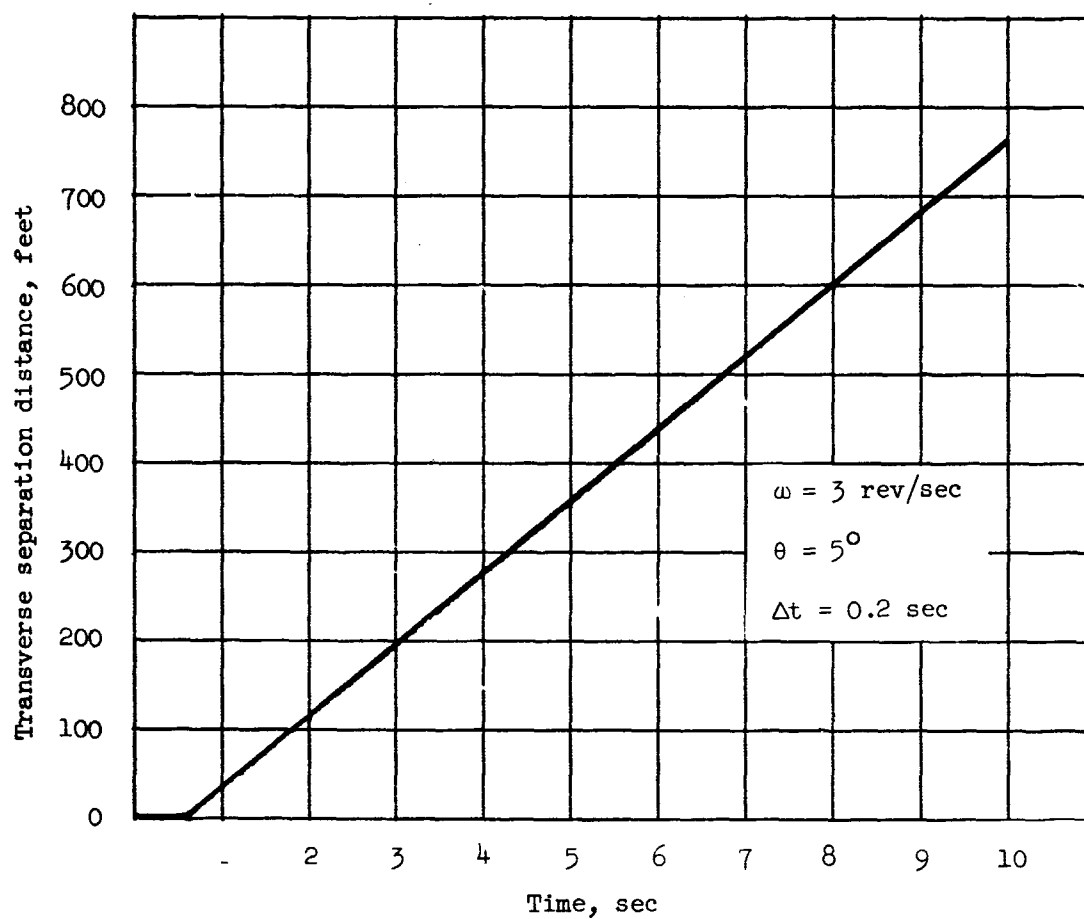


Figure 18.- Lateral separation distance versus time for a motor angle of  $5^\circ$ , spin rate of 3 revolutions per second, and a delay time of 0.2 second.

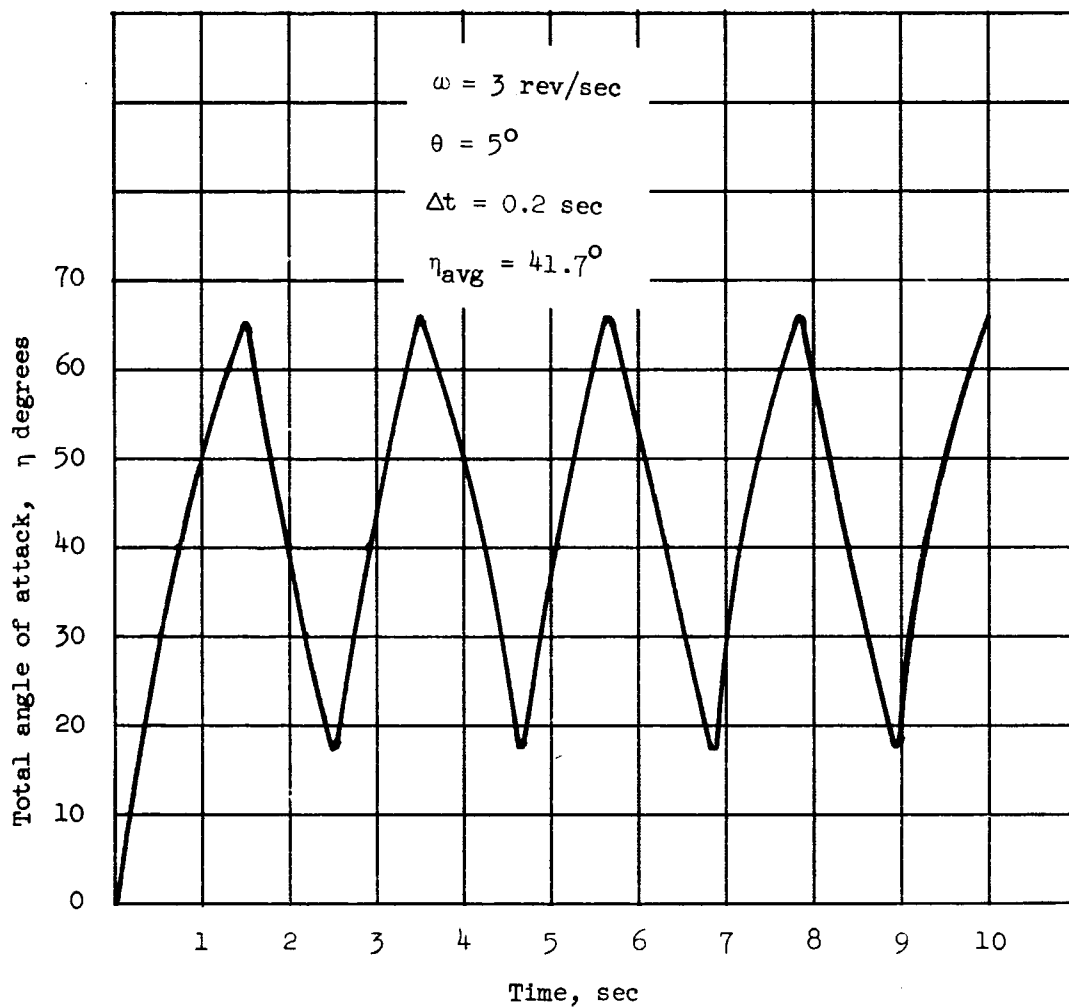


Figure 19.- Total angle of attack versus time for a motor angle of  $5^\circ$ , spin rate of 3 revolutions per second, and a time delay of 0.2 second; vacuum impingement effects considered.



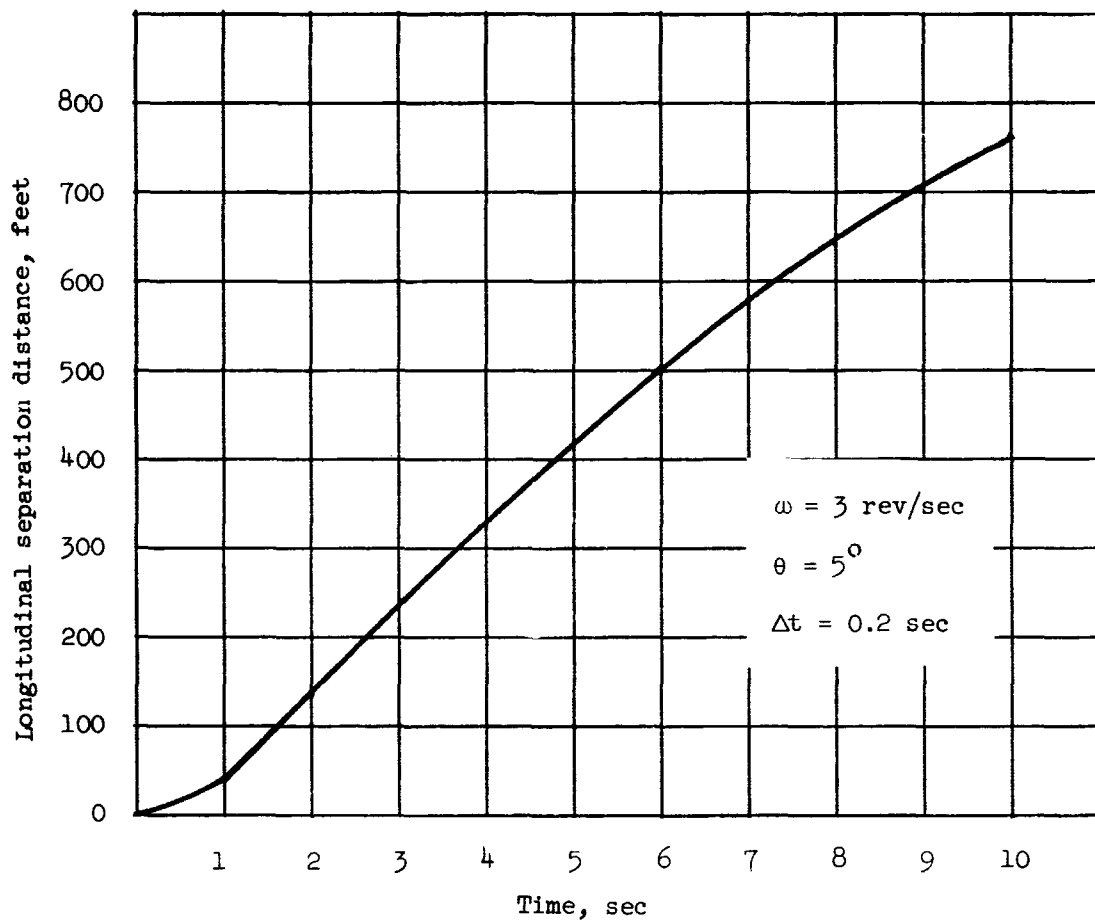


Figure 20.- Longitudinal separation distances versus time for a motor angle of  $5^\circ$ , spin rate of 3 revolutions per second, and a delay time of 0.2 second; vacuum impingement effects considered.

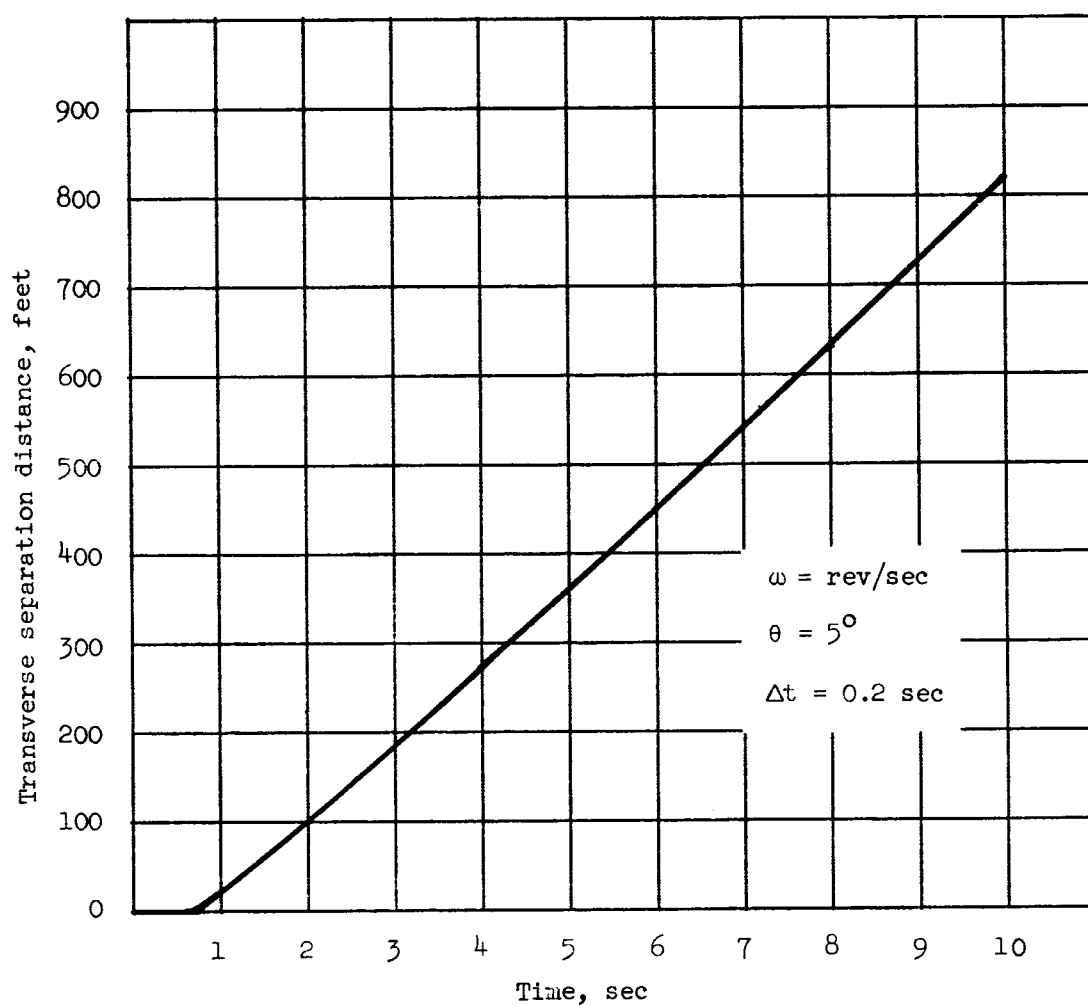


Figure 21.- Lateral separation distances versus time for a motor angle of  $5^\circ$ , spin rate of 3 revolutions per second, and a delay time of 0.2 second; vacuum impingement effects considered.

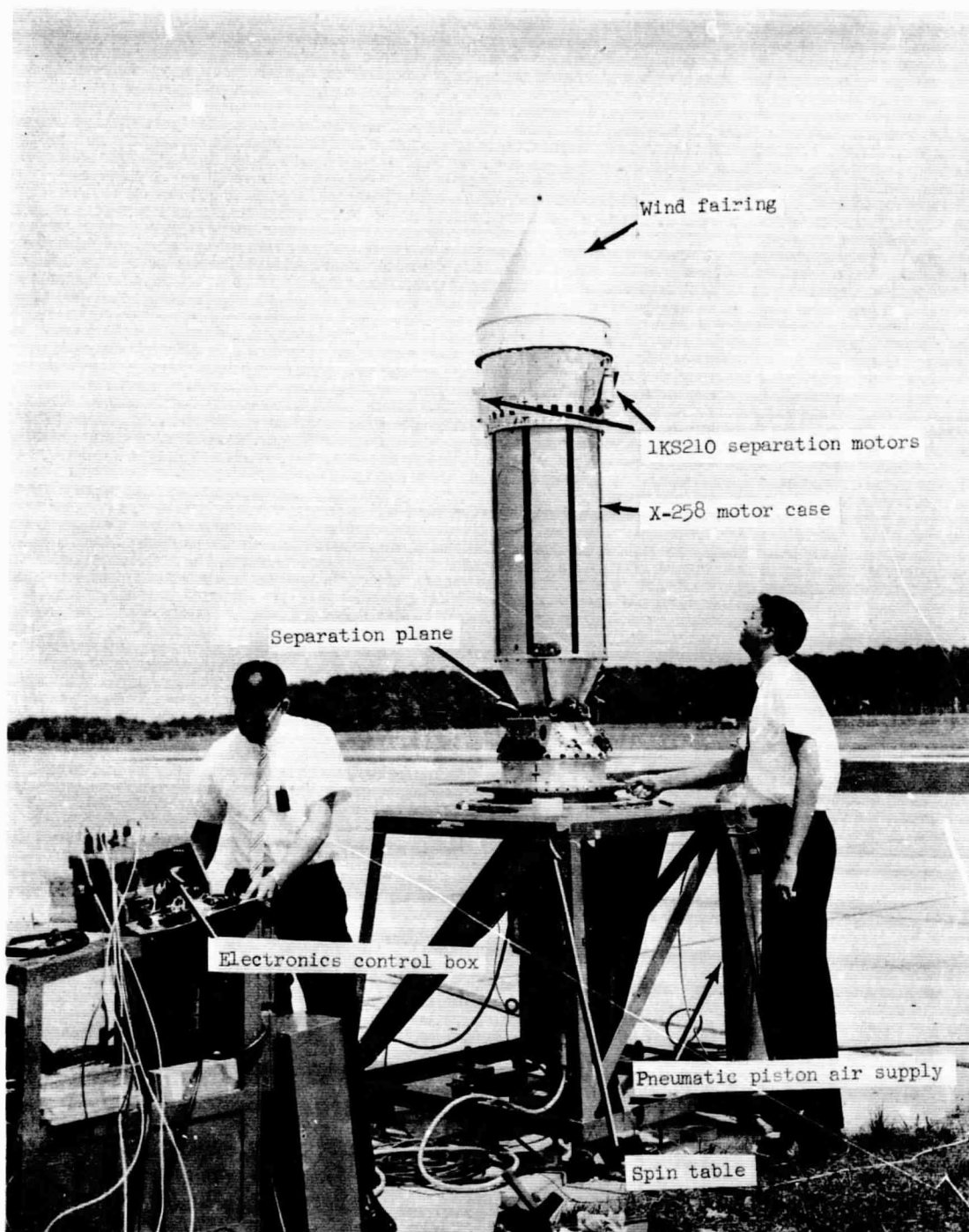


Figure 22.- Separation system verification test setup.